Available online at www.sciencedirect.com

ScienceDirect

Geochimica et Cosmochimica Acta 332 (2022) 239–262

Geochimica et Cosmochimica Acta

www.elsevier.com/locate/gca

Multi-stage evolution of the Lost City hydrothermal vent fluids

Karmina A. Aquino [a,*], Gretchen L. Früh-Green [a], Jörg Rickli [a], Stefano M. Bernasconi [a], Susan Q. Lang [b,1], Marvin D. Lilley [c], David A. Butterfield [d]

[a] Department of Earth Sciences, ETH Zurich, 8092 Zurich, Switzerland
[b] School of the Earth, Ocean, and Environment, University of South Carolina, Columbia, SC 29208, USA
[c] School of Oceanography, University of Washington, Seattle, WA 98195, USA
[d] Cooperative Institute for Climate, Ocean and Ecosystem Studies, University of Washington and NOAA Pacific Marine Environmental Lab, Seattle, WA 98115, USA

Received 22 March 2021; accepted in revised form 22 June 2022; Available online 28 June 2022

Abstract

Serpentinization-influenced hydrothermal systems, such as the Lost City Hydrothermal Field (LCHF), are considered as potential sites for the origin of life. Despite an abundance of reducing power in this system (H_2 and CH_4), microbial habitability may be limited by high pH, elevated temperatures, and/or low concentrations of bioavailable carbon. At the LCHF, the relative contribution of biotic and abiotic processes to the vent fluid composition, especially in the lower temperature vents, remain poorly constrained. We present fluid chemistry and isotope data that suggest that all LCHF fluids are derived from a single endmember produced in the hotter, deeper subsurface essentially in the absence of microbial activity. The strontium isotope composition ($^{87}Sr/^{86}Sr$) of this fluid records the influence of underlying mantle and/or gabbroic rocks, whereas sulfur isotope composition indicates closed-system thermochemical sulfate reduction. Conductive cooling and transport is accompanied by continued sulfate reduction, likely microbial, and mixing with unaltered seawater, which produce second-order vents characterized by higher $\delta^{34}S_{sulfide}$ and lower $\delta^{34}S_{sulfate}$ values. Third-order vent fluids are produced by varying degrees of subsurface mixing between the first- and second-order fluids and a seawater-dominated fluid. Additional biotic and abiotic processes along different flow paths are needed to explain the spatial variability among the vents. Relationships between sulfur geochemistry and hydrogen concentrations dominantly reflect variations in temperature and/or distance from the primary outflow path. Methane concentrations are constant across the field which point to an origin independent of flow path and venting temperature. At Lost City, not all vent fluids appear to have zero Mg concentrations. Thus, we propose an extrapolation to a Sr isotope-endmember composition as an alternative method to estimate endmember fluid compositions at least in similar systems where a two-component mixing with respect to Sr isotopes between seawater and endmember fluids can be established.

Keywords: Serpentinite-hosted hydrothermal systems; Hydrothermal vent fluids; Sulfate reduction; Sr isotope; Sulfur geochemistry

1. INTRODUCTION

Serpentinite-hosted hydrothermal systems are typically associated with significant amounts of electron donors such as H_2 (hydrogen), CH_4 (methane), $HCOO^-$ (formate), and other short-chain organic acids (Charlou et al., 1998, 2002; Kelley et al., 2005; Schmidt et al., 2007; Lang et al.,

* Corresponding author.
E-mail address: karmina.aquino@erdw.ethz.ch (K.A. Aquino).
[1] Present address: Woods Hole Oceanographic Institution, 360 Woods Hole Road, Woods Hole, MA 02543, USA.

https://doi.org/10.1016/j.gca.2022.06.027
0016-7037/

2010; Monnin et al., 2014; Eickenbusch et al., 2019), theoretically providing twice as much energy for microbial chemolithoautotrophy as basalt-hosted systems (McCollom, 2007). These systems are thus often considered as potential sites for the origin of the earliest metabolisms on Earth and other planets (Schulte, et al., 2006; Russell et al., 2010). Yet, despite the presence of abundant reducing power, these systems typically have elevated temperatures, extreme pH, and/or lack bioavailable carbon, which are potential physiological barriers that limit microbial habitability in the absence of substantial mixing with seawater (Lang et al., 2018; Eickenbusch et al., 2019; Lang & Brazelton 2020).

Since its serendipitous discovery in 2000 (Kelley et al., 2001), the Lost City Hydrothermal Field (LCHF) remains one of the most extensively studied serpentinite-hosted hydrothermal systems. LCHF is located on the southern wall of the Atlantis Massif, approximately 15 km west of the Mid-Atlantic Ridge (MAR) at 30°N, near the intersection with the Atlantis Transform Fault (Fig. 1A, B, Table 1). Moderately high temperature (up to 96 °C, Seyfried et al. (2015) measured up to 116 °C), high pH fluids vent from carbonate-brucite chimney structures that tower as high as 60 m above the seafloor (Kelley et al., 2001; Früh-Green et al., 2003; Ludwig et al., 2006; Seyfried et al., 2015). In addition to elevated concentrations of H_2, CH_4, and $HCOO^-$, the vent fluids contain up to ~ 4 mmol/kg of dissolved sulfate (SO_4^{2-}) (Kelley et al., 2005; Proskurowski et al., 2006; Lang et al., 2010), providing energy and carbon sources that drive a microbial ecosystem of methanogenic and methanotrophic archaea, and sulfur-oxidizing and sulfate-reducing bacteria (Schrenk et al., 2004; Brazelton et al., 2006; Gerasimchuk et al., 2010; Lang et al., 2018). Sites that are actively venting high temperature fluids are dominated by the methane-cycling archaea Lost City *Methanosarcinales* (LCMS); while anaerobic methanotrophic archaea (ANME-1) are found in the cooler, more diffusely venting portions of the structures and in inactive chimneys (Schrenk et al., 2004; Brazelton et al., 2006).

Systematic variations in dissolved sulfide (H_2S), SO_4^{2-} and H_2 concentrations (see Section 3.2; Figs. 1C, D, 2; Tables 2, 3) in the vent fluids have been used to suggest that hydrogenotrophic microbial sulfate reduction (MSR) is a major process in the LCHF subsurface (Kelley et al., 2005; Proskurowski et al., 2006; Lang et al., 2012). Moreover, 16S rRNA gene sequencing of chimneys and vent fluids provided evidence for sulfate reducing bacteria at Lost City (Brazelton et al., 2006; Brazelton et al., 2010; Gerasimchuk et al., 2010; Lang et al., 2018). Yet, variations

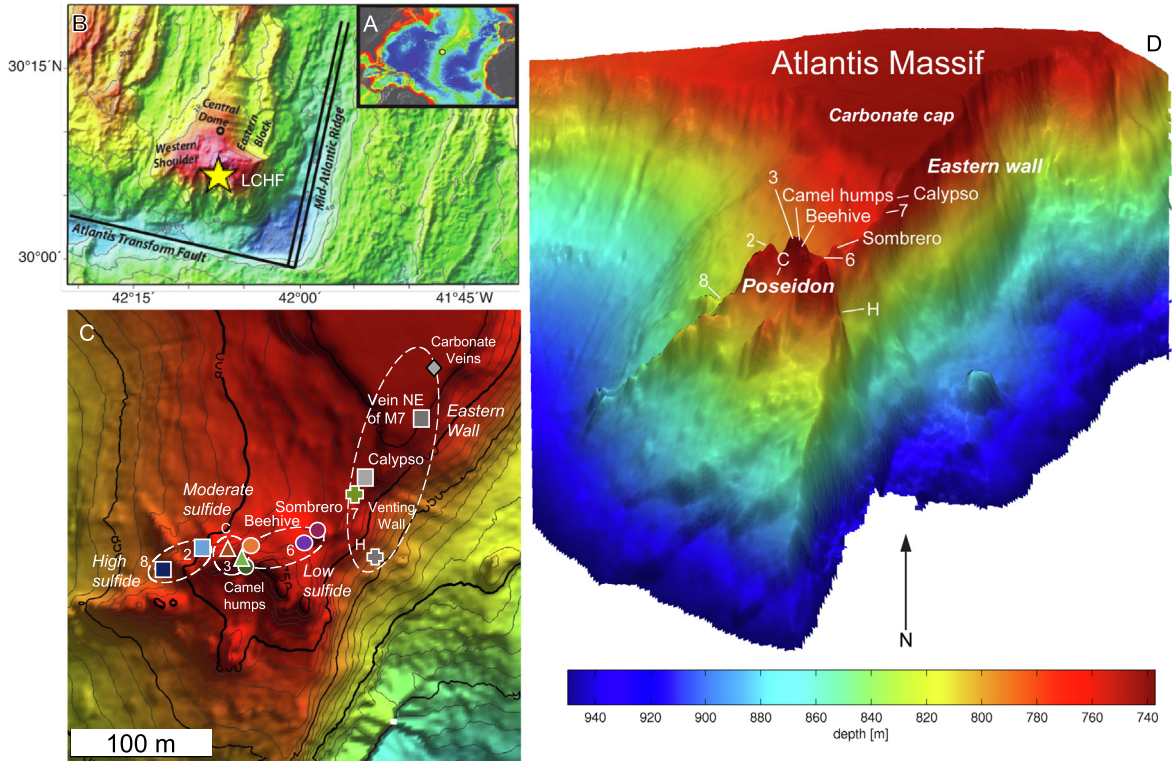

Fig. 1. (A-B) The LCHF is a low-temperature system located at 30°N west of the MAR on the southern wall of the Atlantis Massif. The system is fueled by serpentinization and lithospheric cooling that results in warm, high-pH fluids, rich in hydrogen, methane, and formate. The Atlantis Massif is an oceanic core complex located in the inside corner of the intersection of the MAR and Atlantis Transform Fault. (C) LCHF sites that were included in this study. Sulfur geochemistry and hydrogen concentrations of the vent fluids define four vent groups: low sulfide, moderate sulfide, high sulfide, and eastern wall vents. Symbols correspond to those used in subsequent figures. (D) Three-dimensional view of the LCHF including the location of the vent sites (after Kelley et al., 2005). Massive pinnacles at the summit are composite, actively venting edifices that make up the massive 60 m-tall structure Poseidon.

Table 1
Location of vent sites investigated in this study.

Vent	Latitude	Longitude	Depth (m)
Beehive	30° 7′ 26.1″ N	−42° 7′ 11.9″ W	743
Camel humps	30° 7′ 10.0″ N	−42° 7′ 29.2″ W	732
Marker 6	30° 7′ 14.6″ N	−42° 7′ 26.9″ W	777
Sombrero	30° 7′ 11.0″ N	−42° 7′ 28.0″ W	762
Marker C	30° 7′ 14.6″ N	−42° 7′ 27.6″ W	780
Marker 3	30° 7′ 13.8″ N	−42° 7′ 27.0″ W	730
Marker 2	30° 7′ 13.8″ N	−42° 7′ 27.5″ W	763
Marker 8	30° 7′ 13.7″ N	−42° 7′ 29.7″ W	801
Calypso	30° 7′ 28.6″ N	−42° 7′ 09.6″ W	798
Vein on carbonate cap	30° 7′ 29.8″ N	−42° 7′ 07.7″ W	741
Vein on wall NE of Marker 7	30° 7′ 09.1″ N	−42° 7′ 27.5″ W	864
Background seawater	30° 7′ 47.9″ N	−42° 7′ 20.0″ W	849

in the sulfur geochemistry of serpentinites and gabbros from the southern wall of the Atlantis Massif and near Lost City have been shown to reflect the influence of both microbial and thermochemical sulfate reduction (TSR) (Delacour et al., 2008a,b; Liebmann et al., 2018). Discriminating between MSR and TSR based on the concentration of reaction products alone is difficult, if not impossible (Machel et al., 1995; Machel, 2001). MSR and TSR occur in two mutually exclusive temperature regimes: MSR generally occurs at temperatures below ~ 80 °C (Postgate, 1984); while TSR occurs at temperatures of at least ~ 80–100 °C (Worden et al., 1995; Machel et al., 1995; Machel, 1998; 2001). In addition, reaction rates for TSR are considered geochemically important only at temperatures above 200 °C and low pH (e.g., pH < 4) (Kiyosu, 1980; Ohmoto and Lasaga, 1982). Even though the temperatures of fluids exiting the Lost City chimneys are below the currently known temperature limit of life (122 °C, Takai et al., 2008), the highest measured vent temperature (~116 °C at Beehive, Fig. 1C) and calculated temperatures of reaction in the basement rocks (200 ± 50 °C, Allen, & Seyfried, 2004; Proskurowski et al., 2006; Seyfried et al., 2015) are above the temperature realm of MSR.

Both the vent fluids and basement rocks at Lost City have been shown to be influenced by abiogenic as well as microbial processes. The geochemistry of inorganic and organic carbon in the Atlantis Massif serpentinites is attributed to both abiotic and microbially mediated processes (Delacour et al., 2008c). Recent clumped isotope analyses of CH_4 in the relatively high temperature vent fluids (venting temperatures of > 60^{0}C) suggest that CH_4 is generated abiotically at temperatures > 250^{0}C (Wang et al., 2018; Labidi et al., 2020). δD equilibration in the lower temperature vents and $\Delta^{12}CH_2D_2$ re-equilibration (and partial $\Delta^{13}CH_3D$ re-equilibration) in some of the > 60^{0}C vents, on the other hand, is possibly mediated by microbial activity (Proskurowski et al., 2006; Labidi et al., 2020). Earlier studies have shown that low molecular weight hydrocarbons and the organic acid formate in the vent fluids have abiogenic origins, while acetate is possibly a microbial by-product (Proskurowski et al., 2008; Lang et al., 2010). Although the vent fluid compositions at the LCHF are likely influenced by both biotic and abiotic processes, the relative contribution of these processes is unknown.

Here we present new vent fluid chemistry and isotope data to investigate the origin and fate of sulfur, as well as to constrain fluid flow paths during the relatively low temperature hydrothermal circulation at LCHF. Sulfur isotope data, together with SO_4^{2-}, H_2S, H_2, and CH_4 concentrations of the LCHF vent fluids, confirm previous studies (Allen and Seyfried, 2004; Foustoukos et al., 2008; Lang et al., 2012; Seyfried et al., 2015; Wang et al., 2018; Labidi et al., 2020) suggesting that the highest temperature fluids may be produced in the deeper, hotter serpentinite subsurface in the absence of microbial activity. The compositional variability that we observe in the lower temperature vents points to additional processes in the shallower subsurface or within the porous chimney interiors.

2. METHODS

2.1. Sampling

Fluids were collected with the remotely operated vehicle (ROV) *Jason* during *R/V Atlantis* cruise AT42-01 in 2018. We use vent locality names (Fig. 1, Table 1) that have been established over the course of 20 years of studying Lost City. In some cases, the vents have names inspired by mythology or are descriptive of the structure form, such as Beehive and Sombrero; others are named after field markers set out in 2003 (Kelley et al., 2005). The center of the field is made up of composite, actively venting edifices that form the massive 60-m high structure Poseidon (Kelley et al., 2005; Fig. 1D). We also sampled two carbonate veins in the serpentinite basement where active venting was observed. The first vein is located NE of Marker 7, and the second is a thick vein that cuts the carbonate cap sedimentary sequences at the top of the massif (Kelley et al., 2001) and is named "vein on carbonate cap". Not all vent structures investigated in 2003 could be sampled again in 2018 (such as the Markers 7 and H vents), while Camel Humps, Calypso, and Sombrero were sampled for the first time in 2018. Vent fluids were collected using a custom-built high-volume fluid sampler (referred to as the Hydrothermal Organic Geochemistry or HOG sampler; Lang and Benitez-

Table 2
Measured and endmember compositions of the LCHF vent fluids. Endmember concentrations were determined by extrapolating the measured values to an endmember Sr abundance and $^{87}Sr/^{86}Sr$ value, while endmember isotopic compositions were calculated using isotope mass balance involving $\%SW_{Sr}$. Mg, SO_4^{2-}, H_2S and stable isotope data are obtained from the HOG samples (except for Marker 6 data which are obtained from the major samples). Also shown are corresponding fraction of seawater obtained from Mg ($\%SW_{Mg}$ = measured Mg/seawater Mg × 100%) and Sr isotopes (Eq. A(2)) and △SW (= $\%SW_{Mg}$ - $\%SW_{Sr}$).

Vent	Dive - Time	T_{max}	pH@T_{max}	pH @22 °C	Mg	Sr	$^{87}Sr/^{86}Sr$	SO_4^{2-}	H_2S	$\delta^{18}O$	$\delta^{34}S_{sulfate}$	$\delta^{34}S_{sulfide}$	$\%SW_{Mg}$	$\%SW_{Sr}$	△SW
Low sulfide vents															
Beehive	1108–0606	95.7		10.8	0.1	0.092	0.70649	3.4	0.3	0.3	31.9	29.1	0.2 ± 0.0	0.0 ± 0.1	0.2
	1108–0536	95.7		10.7	1.9	0.092	0.70657	4.0	0.3	0.5	29.3	28.5	3.5 ± 0.1	3.2 ± 0.6	0.3
	1108–0546	95.4		10.8	0.9	0.092	0.70653	3.6	0.3	0.5	31.1	28.7	1.7 ± 0.1	1.0 ± 0.4	0.7
	1108–0556	95.6		10.8	0.4	0.092	0.70654	3.6	0.3	0.4	31.3	28.1	0.7 ± 0.0	1.2 ± 0.4	−0.5
	Endmember		8.9	10.8	0.1	[a]0.092	0.70650	3.3	0.3	0.4	31.0	28.6			
Camel	1111–0440	85.0		9.0	26.6	0.087	0.70770	14.7	0.1	0.2	23.0	28.4	49.5 ± 1.5	48.1 ± 0.6	1.4
Humps	1111–0449	85.0		9.8	13.4	0.089	0.70709	9.0	0.2	0.3	24.8	nd	25.0 ± 0.8	24.4 ± 0.5	0.6
	Endmember		7.9	9.2	0.7	0.092	0.70650	2.4	0.3	0.4	25.5	28.4			
Marker 6	1112-Major 1	65.8		10.6	4.8	0.091	nd		0.4	nd	nd	nd	8.9 ± 0.3	[b]2.2 ± 0.1	6.7
	1112-Major 2	65.8		10.2	13.0	0.089	nd		0.3	nd	nd	nd	24.2 ± 0.7	[b]18.6 ± 0.3	5.6
	Endmember		9.3	10.6	[a]3.7	0.092			0.4						
Sombrero	1111–2334	61.6		9.1	25.7	0.088	0.70759	14.3	0.2	0.2	22.7	30.3	47.8 ± 1.4	43.5 ± 0.6	4.3
	1111–2306	56.8		9.1	25.2	0.087	0.70757	14.1	0.2	0.2	23.5	30.1	46.9 ± 1.4	43.1 ± 0.6	3.8
	1111–2315	56.7		9.2	24.1	0.088	0.70751	13.5	0.2	0.2	23.1	28.6	44.9 ± 1.3	40.9 ± 0.5	4.0
	1111–2325	58.5		9.3	21.8	0.087	0.70741	12.6	0.2	0.2	23.5	31.4	40.6 ± 1.2	36.5 ± 0.5	4.1
	Endmember		8.3	9.2	3.7	0.092	0.70650	3.1	0.4	0.4	24.7	30.1			
Moderate sulfide vents															
Marker C	1110–2212	79.7		10.1	5.9	0.090	0.70677	5.6	0.8	0.2	26.1	31.8	10.9 ± 0.3	11.3 ± 0.5	−0.4
	1110–2140	80.6		10.1	6.3	0.089	0.70679	5.7	0.9	0.3	26.4	31.3	11.7 ± 0.4	11.9 ± 0.6	−0.2
	1110–2152	80.0		10.0	11.1	0.088	0.70702	7.7	0.8	0.2	24.8	31.9	20.7 ± 0.6	21.0 ± 0.5	−0.3
	1110–2202	79.6		10.0	9.3	0.089	0.70692	7.2	0.8	0.3	25.9	32.0	17.4 ± 0.5	17.4 ± 0.5	0.0
	Endmember		8.6	10.1	0.0	0.092	0.70650	2.6	1.0	0.3	26.6	31.8			
Marker 3	1107–1330	45.0		9.4	29.7	0.089	0.70787	16.8	nd	0.3	22.5	30.3	55.3 ± 1.7	53.1 ± 0.6	2.2
	1107–1344	44.5		9.2	32.5	0.089	0.70800	18.1	0.5	0.3	22.5	30.3	60.5 ± 1.8	57.8 ± 0.6	2.7
	1107–1357	55.1		9.3	28.2	0.088	0.70780	15.4	0.6	0.3	22.8	30.8	52.4 ± 1.6	50.8 ± 0.6	1.6
	Endmember		9.1	10.1	2.5	0.092	0.70650	2.6	1.2	0.6	24.5	30.5			
High sulfide vents															
Marker 2	1107–1951	61.5		10.0	23.4	0.088	0.70758	13.2	nd	0.4	22.6	32.3	43.5 ± 1.3	43.4 ± 0.6	0.1
	1107–2006	62.4		10.2	5.7	0.095	0.70682	4.6	2.3	0.3	23.7	32.4	10.6 ± 0.3	9.9 ± 0.4	0.8
	1107–2016	63.9		10.2	3.1	0.095	0.70671	3.4	2.4	0.3	25.3	32.3	5.7 ± 0.2	4.9 ± 0.3	0.8
	1107–2025	58.3		10.1	21.8	0.088	0.70753	11.8	1.8	0.3	21.7	32.3	40.6 ± 1.2	41.4 ± 0.6	−0.9
	Endmember		9.0	10.0	0.3	0.092	0.70650	1.7	2.6	0.5	23.9	32.3			

Marker 8	1110–0312	53.8		10.0	12.0	0.089	0.70707	7.3	2.6	0.1	23.3	32.6	22.3 ± 0.7	21.6 ± 0.5	0.6
	1110–0336	52.6			14.5	0.087	0.70719	8.5	2.5	0.2	22.3	32.6	26.9 ± 0.8	25.9 ± 0.5	1.0
	Endmember		9.4	9.2	0.7	0.092	[c]0.70656	1.5	3.4	0.2	23.4	32.6			
Eastern wall sites															
Calypso	1108–1853	31.8		9.3	33.3	0.086	0.70797	17.6	1.0	0.2	21.6	31.5	62.0 ± 1.9	58.1 ± 0.7	3.9
	1108–1813	26.2		9.3	36.3	0.085	0.70812	19.0	0.9	0.2	20.8	31.1	67.6 ± 2.0	63.2 ± 0.7	4.3
	1108–1822	26.2		9.3	34.3	0.085	0.70803	18.2	0.6	0.2	21.2	31.4	63.8 ± 1.9	59.6 ± 0.7	4.2
	1108–1834	31.8		9.3	35.3	0.084	0.70810	0.0	0.9	0.2	21.2	31.6	65.7 ± 2.0	62.3 ± 0.6	3.5
	1108–1843	32.9		9.4	31.4	0.085	0.70786	16.6	1.1	0.2	21.5	31.5	58.4 ± 1.8	53.1 ± 0.6	5.3
	Endmember		9.4	9.2	5.8	0.092	0.70650	2.6	2.2	0.6	21.6	31.4			
Vein on carbonate cap	1109–0938	10.7	10.1	8.0	53.5	0.082	0.70913	28.3	bdl	0.1	21.4	nd	99.6 ± 3.0	98.6 ± 1.0	1.0
Vein on wall NE of Marker 7	1111–1143	22.0	9.5	9.1	36.6	0.084	0.70814	19.0	0.9	0.1	21.8	31.4	68.1 ± 2.0	63.9 ± 0.8	4.1
	Endmember				6.8	0.092	0.70650	1.8	2.4	0.5	23.2	31.4			
Seawater	1109–1915	11.0		6.4	53.7	0.082	0.70917	28.6	bdl	−0.1	21.4		99.9 ± 3.0	100.0 ± 0.8	−0.1
Seawater	1109–1922	11.0		6.4	53.8	0.082	0.70917	28.6	bdl	0.0	21.3		100.1 ± 3.0	100.2 ± 0.9	−0.1

Concentrations are given in mmol/kg, vent temperatures in ° C, $\delta^{34}S$ in ‰ VCDT, and $\delta^{18}O$ in ‰ VSMOW. The estimated precision of the analyses is 3% for Mg and Sr, 2% for SO_4^{2-}, 4% for H_2S (all as relative standard deviation), and 0.00001 for $^{87}Sr/^{86}Sr$ (standard deviation).

nd = no data or no measurement made.

bdl = below detection limit of analysis.

[a] calculated by fitting measured Sr concentrations in a York regression (Reed, 2010).

[b] No $^{87}Sr/^{86}Sr$ measurements were done for Marker 6. Endmember Mg were calculated from the gas tight sample J1112-GT16. $\%SW_{Sr}$ for the major samples are then calculated from the $\%SW_{Mg}$ taking into account the endmember Mg for this vent.

[c] This value is calculated specifically for Marker 8. If an endmember composition of 0.70650 is used, $\%SW_{Mg} < \%SW_{Sr}$, which suggests from Eq. A(2) that this vent has a slightly higher endmember $^{87}Sr/^{86}Sr$ endmember composition.

Table 3
Measured and endmember compositions of the LCHF gas-tight samples. Also shown are fraction of seawater obtained from Mg and Sr isotopes and △SW (= $\%SW_{Mg}$ - $\%SW_{Sr}$).

Vent	Dive - GT No.	T_{max}	Mg	Sr	$^{87}Sr/^{86}Sr$	H_2	CH_4	$\%SW_{Mg}$	$\%SW_{Sr}$	△SW
Beehive	1108-GT17	95.7	1.4	0.093	0.70653	9.4 ± 0.5	1.1 ± 0.1	2.6% ± 0.1%	1.3% ± 0.7%	1.4%
	Endmember (Mg)					9.6 ± 0.5	1.1 ± 0.1			
	Endmember (Sr)					9.5 ± 0.5	1.1 ± 0.1			
Camel Humps	1111-GT11	85.0	43.8	0.078	0.70856	2.0 ± 0.1	0.2 ± 0.0	81.5% ± 2.4%	79.6% ± 0.9%	1.9%
	Endmember (Mg)					10.8 ± 2.3	1.3 ± 0.3			
	Endmember (Sr)					9.8 ± 1.6	1.1 ± 0.2			
Marker 6	1112-GT16	65.8	28.4	nd	0.70775	6.6 ± 0.3	0.8 ± 0.0	52.8% ± 1.6%	50.2% ± 0.7%	2.6%
	1112-GT5		45.5	0.066	0.70847	2.3 ± 0.1	0.3 ± 0.0	84.71% ± 2.5%	76.1% ± 1.1%	8.6%
	1112-GT17		44.9	0.080	0.70860	1.9 ± 0.1	0.2 ± 0.0	83.5% ± 2.5%	80.8% ± 0.8%	2.8%
	Endmember (Mg)					14.3 ± 0.7	1.6 ± 0.1			
	Endmember (Sr)					13.0 ± 0.9	1.5 ± 0.1			
Sombrero	1109-GT16	61.6	47.8	0.083	0.70882	1.1 ± 0.1	0.2 ± 0.0	89.0% ± 2.7%	88.2% ± 1.0%	0.7%
	1109-GT10		51.9	0.081	nd	0.2 ± 0.0	0.0 ± 0.0	96.6% ± 2.9%	[a]96.4% ± 3.1%	0.2%
	Endmember (Mg)					10.5 ± 2.7	1.5 ± 0.4			
	Endmember (Sr)					9.7 ± 1.3	1.4 ± 0.2			
Marker C	1110-GT18	80.6	8.4	0.091	0.70687	6.9 ± 0.3	1.0 ± 0.0	15.7% ± 0.5%	15.5% ± 0.6%	0.2%
	1110-TGT		22.2	0.087	0.70748	2.9 ± 0.1	0.4 ± 0.0	41.3% ± 1.2%	39.6% ± 0.7%	1.7%
	Endmember (Mg)					7.3 ± 0.5	1.0 ± 0.1			
	Endmember (Sr)					7.2 ± 0.4	1.0 ± 0.1			
Marker 3	1107-GT11	55.1	38.4	0.062	nd	1.2 ± 0.1	0.2 ± 0.0	71.4% ± 2.1%	[a]70.0% ± 2.2%	1.3%
	Endmember (Mg)					4.2 ± 0.6	0.8 ± 0.1			
	Endmember (Sr)					4.1 ± 0.4	0.8 ± 0.1			
Marker 2	1107-GT12	63.9	22.5	0.088	nd	2.1 ± 0.1	0.8 ± 0.0	41.8% ± 1.3%	[a]41.5% ± 1.3%	0.3%
	1111-GT12		0.7	0.090	0.70662	3.1 ± 0.2	1.1 ± 0.1	1.4% ± 0.0%	2.6% ± 0.3%	−1.2%
	1107-GT9		4.6	0.095	0.70656	3.3 ± 0.2	1.2 ± 0.1	8.5% ± 0.3%	5.1% ± 1.3%	3.3%
	Endmember (Mg)					3.4 ± 0.2	1.2 ± 0.1			
	Endmember (Sr)					3.4 ± 0.2	1.2 ± 0.1			
Marker 8	1110-GT9	53.8	25.6	0.085	0.70754	1.5 ± 0.1	0.8 ± 0.0	47.6% ± 1.4%	40.4% ± 0.6%	7.3%
	1110-GT17		37.3	0.078	0.70827	0.8 ± 0.0	0.4 ± 0.0	69.3% ± 2.1%	68.5% ± 0.9%	0.9%
	Endmember (Mg)					2.9 ± 0.3	1.5 ± 0.1			
	Endmember (Sr)					2.6 ± 0.2	1.3 ± 0.1			
[b]*Endmember (Mg)*										
Low sulfide vents					9.7 ± 0.5	1.1 ± 0.1				
Moderate sulfide vents					7.6 ± 0.4	1.1 ± 0.1				
High sulfide vents					3.3 ± 0.2	1.2 ± 0.1				

Concentrations are given in mmol/kg and vent temperatures in ° C. The estimated precision of the analyses is 3% for Mg and Sr, 5% for H_2 and CH_4, (all as relative standard deviation), and<0.00002 for $^{87}Sr/^{86}Sr$ (standard deviation).
nd = no data or no measurement made.
[a] No $^{87}Sr/^{86}Sr$ measurements were done for these samples. $\%SW_{Sr}$ are calculated from the $\%SW_{Mg}$ taking into account the endmember Mg for this vent.
[b] Calculated from data from Proskurowski et al., 2006 and this study.

Nelson, 2021) and standard titanium major samplers (~750 ml; Von Damm et al., 1985) mounted on the ROV *Jason* (Table 2). Samples for volatile analyses were collected using conventional (~150 ml) and a large volume (~1500 ml, referred to as Titan) gas-tight samplers (Table 3). Temperatures were measured using an in-situ temperature probe connected to the HOG sampler's titanium intake nozzle. Upon arrival on deck, sample aliquots were analyzed for pH, alkalinity, dissolved silica, and H_2S. Fluid subsamples for stable isotope analyses were immediately stored at 4 °C.

2.2. Analytical methods

We analyzed a total of 32 HOG samples, including two background seawater samples collected near IODP Borehole M0072B (Früh-Green et al., 2018), for Mg and S concentrations, and O, S, and Sr ($^{87}Sr/^{86}Sr$) isotope compositions. H_2 and CH_4 concentrations were analyzed on 15 gas-tight samples, 12 of which were also measured for $^{87}Sr/^{86}Sr$ ratios. Sr, Mg, and H_2S concentrations were analyzed at the NOAA Pacific Marine Environmental Laboratory using the methods described in Butterfield & Massoth (1994). SO_4^{2-} concentrations were measured using a Dionex Aquion ion chromatography system (ThermoFischer Scientific, Bremen) at the Department of Earth Sciences, ETH Zurich. The estimated precision (1σ) of these analyses are 3% (Mg and Sr), 2% (SO_4^{2-}), and 4% (H_2S). Volatiles were vacuum extracted from the vent fluids and sealed in gas ampoules on board ship and analysed for H_2 and CH_4 concentrations at the University of Washington following the methodology described in Proskurowski et al. (2008). The overall precision of the dissolved volatile analyses is estimated to be about 5%. Calculations of pH at in-situ temperatures were made using the Geochemist Workbench® 14th edition SpecE8 program (Bethke et al., 2020). This was done by first correcting the measured pH for seawater contributions and modelling the corrected vent fluid compositions and pH to the highest measured temperatures for each vent site.

For oxygen isotope analysis, 2 ml of vent fluids were transferred into 12-ml exetainers and flushed with 2% CO_2 in He, stirred and allowed to equilibrate for 24 h following the methods of Epstein & Mayeda (1953). The analyses were conducted using a GasBench II coupled with a Delta V isotope ratio mass spectrometer (IRMS, both ThermoFischer Scientific, Bremen) at the Geological Institute, ETH Zurich. The procedure was calibrated using waters with $\delta^{18}O$ values of + 1.55‰ and −11.01‰, respectively, which were calibrated against the international standards VSMOW and VSLAP. Reproducibility of the measurements is ± 0.1‰.

Samples for sulfur isotope analysis were collected in 50-ml falcon tubes and spiked with 0.5 ml of a 0.4 M cadmium acetate solution to precipitate sulfide. The solutions were centrifuged at 4000 rpm for 30 min to separate the sulfide fraction. To precipitate the sulfate fraction, 1.8 M $BaCl_2$-ś$2H_2O$ solution was added to the supernatant upon acidification to a pH of about 3–4 with 5% HCl. The solutions were then centrifuged for 30 min to collect the barium sulfate. The S isotope compositions were measured in an elemental analyzer coupled to a Thermo-Fisher Delta V isotope ratio mass spectrometer (EA-IRMS). The system was calibrated using international standards NBS-127 ($\delta^{34}S$ = +20.3‰ VCDT) and IAEA-SO-5 ($\delta^{34}S$ = +0.5‰ VCDT) for sulfate, and IAEA-S-1 ($\delta^{34}S$ = −0.30‰ VCDT), IAEA-S-2 ($\delta^{34}S$ = +22.7‰ VCDT), and IAEA-S-3 ($\delta^{34}S$ = –32.3‰ VCDT) for sulfide, with a reproducibility of 0.28‰.

Strontium isotope analysis was conducted on a multicollector-inductively coupled plasma mass spectrometer (Neptune Plus, ThermoFischer Scientific, ETH Zurich) upon isolation of 500 ng of the element using Sr spec resin (Deniel & Pin, 2001; de Souza et al., 2010) in about 3 ml of 2% HNO_3. Instrumental mass fractionation was corrected using the exponential law and a $^{86}Sr/^{88}Sr$ ratio of 0.11940 (Nier, 1938). Sample $^{87}Sr/^{86}Sr$ ratios were renormalized to the accepted value of Nist SRM 987 ($^{87}Sr/^{86}Sr$ = 0.710248, Thirlwall, 1991). External errors estimated from repeated Nist SRM 987 measurements during the three sessions corresponded to < 24 ppm (2 SD, SRM 978 was run at least 15 times per session).

3. RESULTS

3.1. Measured vent fluid compositions

Measured sulfur concentrations and isotope compositions of the Lost City vent fluids are presented in Tables 2 and 3 and plotted in Fig. 2. Measured SO_4^{2-} values range from 3.4 to 28.3 mmol/kg, roughly reflecting mixing between seawater and endmember vent fluids with concentrations similar to or less than that of Beehive (Fig. 2A, B). Measured H_2S values are between 0.1 and 2.6 mmol/kg and reflect mixing between seawater and Beehive, Marker C, or Marker 2 endmember fluids (Fig. 2C). Although there is significant scatter, measured $\delta^{34}S_{sulfate}$ values also roughly reflect mixing between Beehive endmember fluids and seawater (Fig. 2D). Beehive vent fluids have the highest $\delta^{34}S_{sulfate}$ values (+29.3 to + 31.9‰) which decrease in the other vents to seawater sulfate values (+21‰, Rees et al., 1978) with increasing Mg and $^{87}Sr/^{86}Sr$. Measured $\delta^{34}S_{sulfide}$ values are lowest at Beehive (+28.1 to + 29.1‰) and highest at Marker 8 (+32.6‰) and do not show any trend with Mg (Fig. 2E). The samples from the vein on carbonate cap have seawater sulfur chemistry and isotope compositions.

3.2. Endmember sulfur, hydrogen, and methane compositions

Endmember compositions presented here were estimated by using Sr isotopes (see Appendix A). These are presented in Tables 2 and 3 and in Figs. 3 and 4. The endmember sulfur and hydrogen compositions vary systematically with temperature and distance from the center of the field (Figs. 3, 4A, B). Endmember H_2S compositions are between 0.3 and 3.4 mmol/kg and increase with decreasing temperature and H_2 (Figs. 3A, 4A). In contrast, endmember SO_4^{2-} concentrations range from 1.5 to 3.3 mmol/kg and generally increase with temperature and H_2

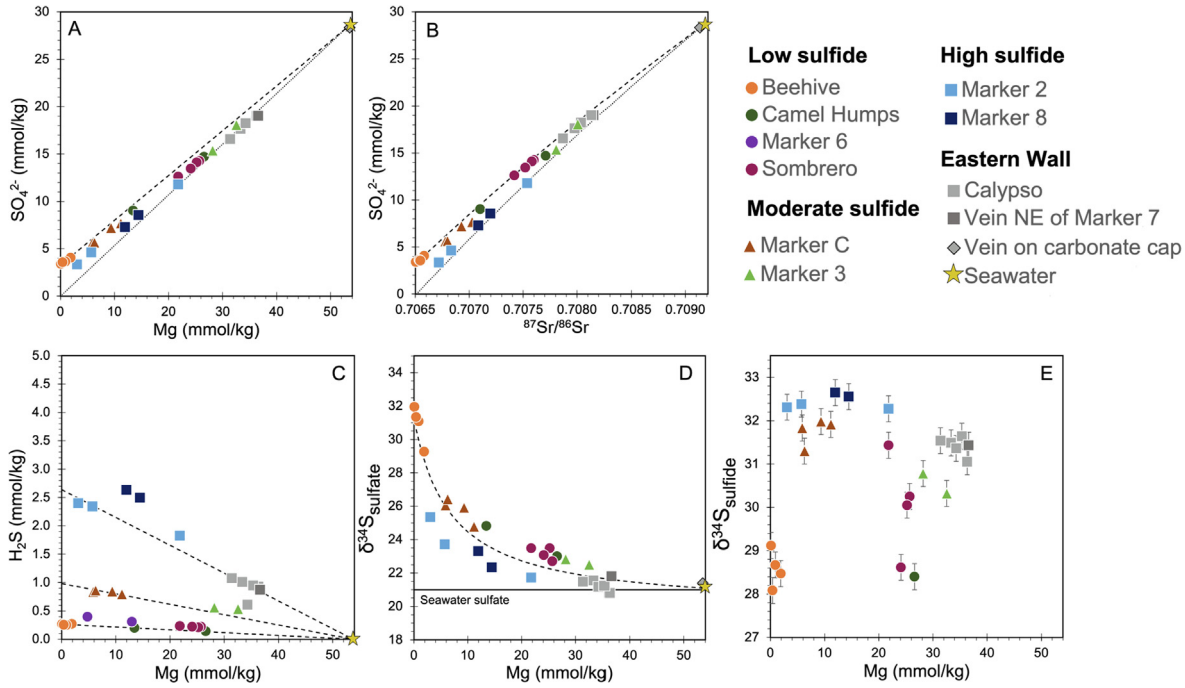

Fig. 2. Measured sulfur concentration and isotope compositions of the Lost City vent fluids. Sulfate concentrations vs. Mg (A) and Sr isotope ratios (B). Sulfide concentrations (C) and sulfur isotope compositions of sulfate (D) and sulfide (E) plotted against Mg. Dashed lines are mixing lines between Beehive, Marker C, or Marker 2 endmember fluids and seawater. Dotted lines are mixing lines between seawater and the origin.

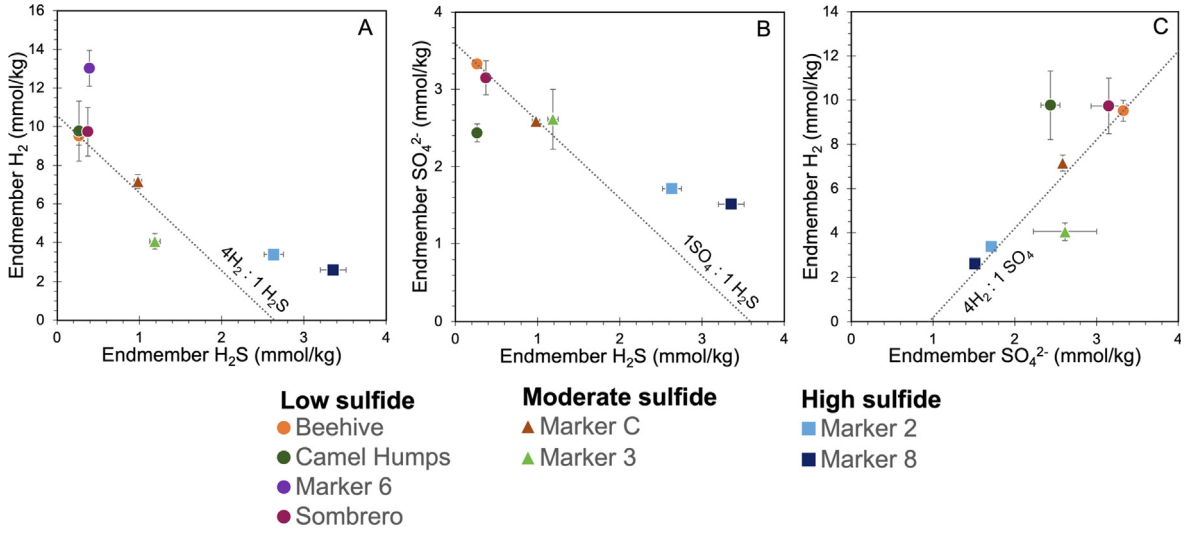

Fig. 3. Endmember concentrations of hydrogen, sulfate, and sulfide in the Lost City vent fluids, calculated using the Sr isotope approach (Appendix A), vary systematically from the central sites (low and moderate sulfide groups) towards the more peripheral sites (high sulfide group). (A) The central sites (low sulfide group) have the lowest sulfide concentrations and high sulfate and hydrogen. Hydrogen and sulfate concentrations decrease towards the lower temperature sites while sulfide concentrations increase. Dotted line shows the expected change in concentrations from Beehive (vent fluid with the highest endmember sulfate concentration) based on the stoichiometry of sulfate reduction (Equation (1)). This systematic variation has been previously used to suggest that microbial sulfate reduction is a major control in the vent fluid compositions (Kelley et al., 2005; Proskurowski et al., 2006; Lang et al., 2012).

(Figs. 3B, C, 4B). Dissolved volatile concentrations (Table 3) are 2.6–13.0 mmol/kg for H_2 and 0.8–1.5 mmol/kg for CH_4. The range of endmember concentrations of the samples collected in 2018 are generally consistent with previously reported values (Table 4; Proskurowski et al., 2006; 2008; Lang et al., 2012; Reeves et al., 2014; Konn et al., 2015;

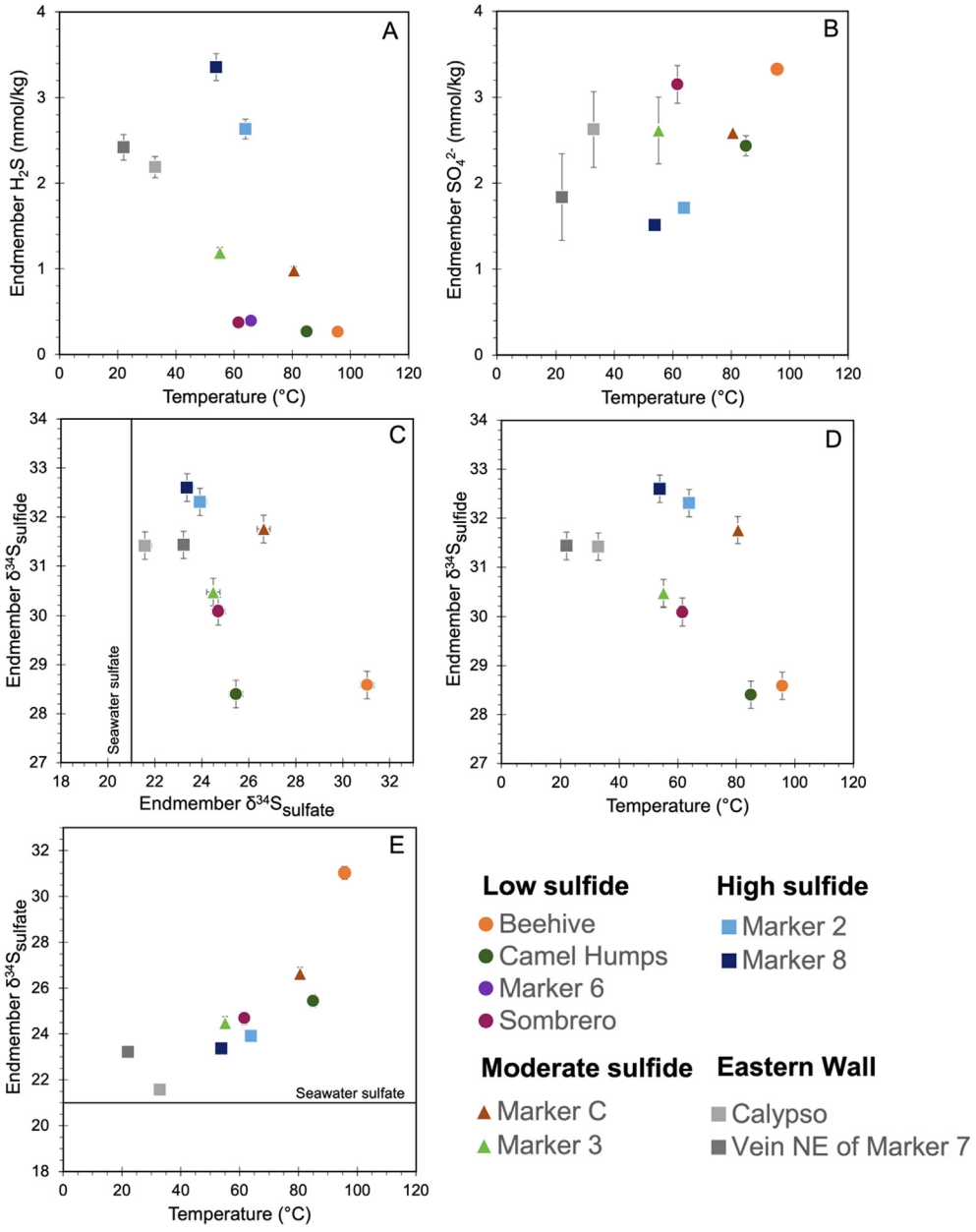

Fig. 4. Variations in the sulfur geochemistry of the LCHF vent fluids with temperature. (A) H_2S increase and (B) SO_4^{2-} decrease with decreasing temperature. (C) Both $\delta^{34}S_{sulfide}$ and $\delta^{34}S_{sulfide}$ are distinctly higher than seawater sulfate, with $\delta^{34}S_{sulfide} > \delta^{34}S_{sulfate,}$ except for Beehive. (D) Endmember $\delta^{34}S_{sulfide}$ increases with decreasing temperature. (E) In contrast, endmember $\delta^{34}S_{sulfate}$ decreases with decreasing temperature, with $\delta^{34}S_{sulfate}$ approaching seawater sulfate values as temperature decreases.

Table 4
Comparison of reported endmember sulfur, methane, and hydrogen concentrations at the LCHF.

	SO_4^{2-}	H_2S	H_2	CH_4	Vents investigated
This study	1.5 to 3.3	0.3 to 3.4	2.6 to 13.0	0.9 to 1.5	see Table 2
Proskurowski et al. (2006, 2008)			0.5 to 14.4	0.9 to 2.0	BH, 2, 3, 6, 7, 8, C, H
Lang et al. (2012)	1.0 to 3.7	0.2 to 2.9			BH, 2, 3, 6, 7, 8, C, H
Reeves et al. (2014)		0.2 to 0.3	10.4 to 10.5	1.1	BH, 6
Konn et al. (2015)			7.8	0.9	BH
Seyfried et al. (2015)[a]	3.2 to 3.5	0.1 to 0.2	9.9 to 10.8	1.2 to 1.3	BH, 6

Concentrations are given in mmol/kg. Note: BH = Beehive; numbers and letters = Marker numbers from Kelley et al. (2005).
[a] Endmember defined as fluid with lowest Mg concentrations.

Seyfried et al., 2015), which shows that compositions at LCHF have remained relatively stable for more than a decade.

The active vents can be subdivided into four groups based largely on location and endmember SO_4^{2-}, H_2S, and H_2 concentrations:

(i) Low sulfide vents,
(ii) Moderate sulfide vents,
(iii) High sulfide vents, and the
(iv) Eastern wall vents.

The low sulfide vents are located at the center of the main field on the Poseidon structure extending towards the eastern wall and include Beehive, Camel Humps, Sombrero, and Marker 6 (Fig. 1C). They have the lowest H_2S (0.3–0.4 mmol/kg), highest SO_4^{2-}, (2.4–3.3 mmol/kg), and highest H_2 endmember concentrations (9.5–13.0 mmol/kg) (Tables 2, 3, Fig. 3). Venting from Beehive is the most vigorous, with the highest temperature fluid (96 °C) that is the most representative of the unaltered, pristine endmember vent fluid at Lost City. H_2 concentrations in this group lie within a narrow range (between 9.5 and 9.8 mmol/kg) except for Marker 6 with endmember H_2 concentration as high as 13.0 mmol/kg (Table 3, Fig. 3). The moderate sulfide group encompasses vents at Marker C and Marker 3, located in the central part of the field on Poseidon. Despite their proximity, the moderate sulfide group has higher H_2S (1.0–1.2 mmol/kg), lower SO_4^{2-} (2.6 mmol/kg), lower H_2 (4.1–7.2 mmol/kg), and generally lower temperatures than the low sulfide group. The high sulfide vents are located in the western part of the field and consist of Marker 2 and Marker 8, both of which have generally lower temperatures (54–64 °C), low SO_4^{2-} (1.5 – 1.7 mmol/kg), the highest H_2S (2.6–3.4 mmol/kg), and the lowest H_2 concentrations (2.6–3.4 mmol/kg) in the LCHF system. The eastern wall is an area with steep basement outcrops just below a northeast trending ridge, north and east of the main vent field towards the top of the Atlantis Massif (Fig. 1). This area is characterized by carbonate veins and variably sized structures that grew directly on the basement serpentinites or along the subhorizontal foliation in the rocks (Kelley et al., 2005). This group includes the Calypso vent, a small chimney located northeast of Marker 7, and a vein sampled on the carbonate cap with diffuse fluids. These vents have lower temperatures (~11–33 °C) compared to those in the main field, high H_2S (2.2–2.4 mmol/kg) and variable SO_4^{2-} concentrations (1.8 – 2.6 mmol/kg).

3.3. Oxygen and sulfur isotope geochemistry

Endmember oxygen isotope compositions of the vent fluids (+0.2 to + 0.6‰) are slightly higher than background seawater (+0.1‰) (Table 2). We observe no general trend in $\delta^{18}O$ with temperature or distance from the center of the field. The highest $\delta^{18}O$ value of + 0.6‰ is observed in Marker 3 and Calypso while the vein NE of Marker 7 and Marker 2 are both at + 0.5‰. Samples from the low sulfide vents have $\delta^{18}O$ values of + 0.4‰. The fluid sample from the vein on the carbonate cap has a $\delta^{18}O$ close to background seawater (+0.1‰).

The endmember $\delta^{34}S$ of sulfate and sulfide in the vent fluids are higher than seawater sulfate ($\delta^{34}S_{sulfate}$: +21‰, Rees et al., 1978), with $\delta^{34}S_{sulfate}$ values ranging from + 21.6 to + 31.0‰, and $\delta^{34}S_{sulfide}$ from + 28.4 to + 32.6‰ (Table 2, Fig. 4C-E). $\delta^{34}S_{sulfide}$ is more positive than $\delta^{34}S_{sulfate}$ in all vents, except Beehive (Fig. 4C). Moreover, $\delta^{34}S_{sulfide}$ values generally increase with increasing H_2S concentrations and distance from the center of the field, and broadly increase with decreasing vent temperatures (Fig. 4A, D). The $\delta^{34}S_{sulfate}$ values, on the other hand, generally decrease towards seawater $\delta^{34}S_{sulfate}$ values with decreasing vent temperatures and SO_4^{2-} concentrations (Fig. 4B, E). At the eastern wall (Calypso), $\delta^{34}S_{sulfate}$ values are very close to seawater (Fig. 4D).

4. DISCUSSION

4.1. Mixing trends in the LCHF vent fluids

Mixing diagrams, which are plots of measured concentrations, are useful for calculating endmember compositions and determining whether an element behaves conservatively during mixing of seawater with vent fluids. Most of the samples do not lie directly on the Beehive-seawater mixing line when measured SO_4^{2-} compositions are plotted against Mg (Fig. 2A). Instead, some of the lower temperature vent fluids plot along the mixing line with a zero-Mg, zero-sulfate endmember. The sulfate in these fluids are enriched in ^{34}S compared to seawater, requiring that these endmember fluids contain sulfate with a non-seawater $\delta^{34}S_{sulfate}$ value (Fig. 2D). For a non-zero sulfate endmember fluid to plot along the same linear mixing line as a zero-Mg, zero-sulfate endmember, it requires that the fluid also contains a corresponding amount of Mg (Sakai et al., 1990; Gamo et al., 1991; see Appendix A). When measured SO_4^{2-} compositions are plotted against $^{87}Sr/^{86}Sr$ (Fig. 2B), samples from Sombrero, Marker 3, Camel humps, Calypso, and vein NE of Marker 7 move closer to this mixing line, supporting the idea that small amounts of Mg in these vents may move the data points towards a zero-Mg, zero-sulfate endmember (Fig. 2A). Several vents including Markers 2, C, and 8 have measured SO_4^{2-} that are below the mixing line between Beehive-seawater but above the zero-sulfate line when plotted against both $^{87}Sr/^{86}Sr$ and Mg (Table 2, Fig. 2A, B, see Section 3.3), suggesting lower endmember SO_4^{2-} in these vents relative to Beehive.

As shown in Fig. 5, the $^{87}Sr/^{86}Sr$ ratio of the Lost City vent fluids plotted against Mg or Mg/Sr define a mixing line between seawater ($^{87}Sr/^{86}Sr = 0.70917$, Palmer & Edmond, 1989) and a zero-Mg endmember vent fluid with a $^{87}Sr/^{86}Sr$ of 0.70650. The strong correlation between $^{87}Sr/^{86}Sr$ and Mg/Sr ($R^2 = 0.995$) suggests that the LCHF vent fluids were all formed from a primary endmember fluid with $^{87}Sr/^{86}Sr$ close to that sampled at Beehive. In contrast to the Sr isotope vs. Mg/Sr plot (Fig. 5), the sulfur chemistry of the LCHF vent fluids (Fig. 6) define three mixing lines that broadly reflect variations observed in the four vent

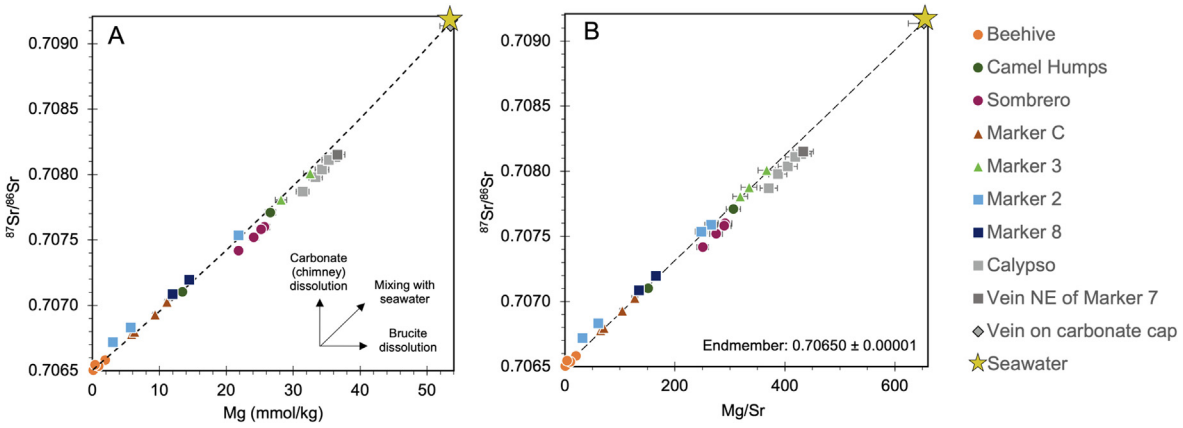

Fig. 5. Measured $^{87}Sr/^{86}Sr$ vs. (A) Mg and (B) Mg/Sr plots of the LCHF vent fluids define mixing lines between seawater ($^{87}Sr/^{86}Sr$ = 0.70917) and an endmember vent fluid with $^{87}Sr/^{86}Sr$ of 0.70650. Also shown are the effects (black arrows) of multiple processes to the endmember fluids. Dissolution of carbonate chimneys will increase the $^{87}Sr/^{86}Sr$ while dissolution of brucite will increase the Mg concentrations of the fluids, in excess of what can be explained by mixing with seawater. Sombrero, Marker 3, and Calypso have measured Mg slightly in excess of what is expected from mixing with seawater Mg, which may hint to a non-zero endmember Mg in these vents.

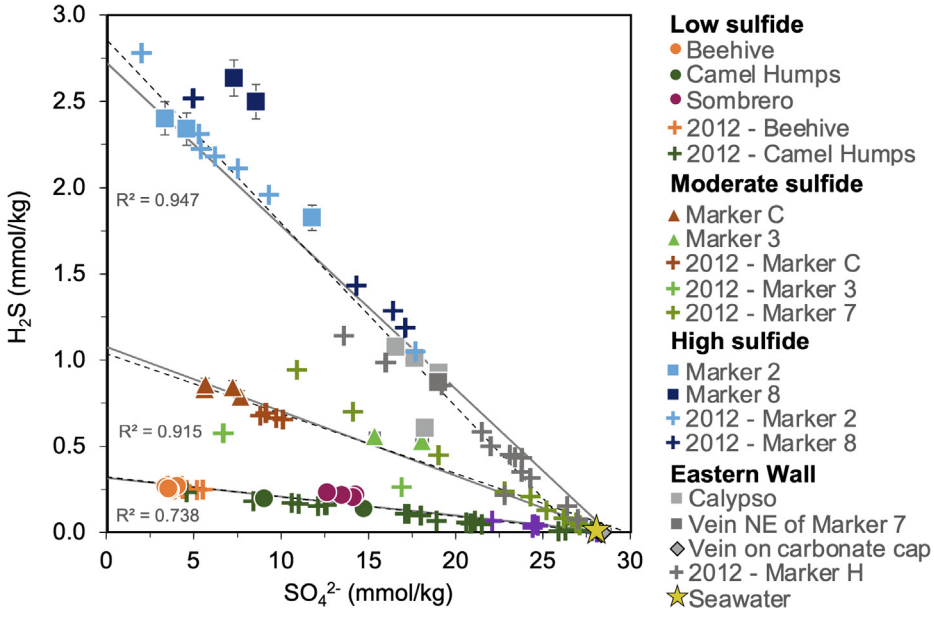

Fig. 6. Plot of measured H_2S against sulfate of the LCHF vent fluids, which defines three mixing lines between a high temperature, high sulfide, and low sulfate endmember vent fluid and a fluid with sulfur chemistry similar to seawater. Each mixing line roughly corresponds to the vent groupings discussed in the text. Symbols indicated as crosses (+) are data from Lang et al. (2012). Dark solid lines are mixing lines expected from mixing between the highest temperature fluid within each group and seawater with 28 mmol/kg of sulfate (and 0 mmol/kg H_2S). Dashed lines are regression lines obtained from the vent chemistry data for each group.

groups defined in Section 3.2. Within each group, the sulfur chemistry can be explained by mixing between the highest temperature vent and a fluid close to seawater. The sulfur chemistry of the low sulfide vents can be explained by mixing between seawater and an endmember fluid best represented by Beehive, while the moderate sulfide vents can be explained by mixing between seawater and an endmember fluid with the composition of Marker C. Similarly, the sulfur chemistry of the high sulfide and eastern wall groups points to mixing between seawater and an endmember fluid best represented by Marker 2 vent fluid. Closer examination of each of these mixing lines reveals that the lower temperature vents slightly deviate from these mixing lines, suggesting that additional processes may influence vent fluid compositions at lower temperatures.

4.2. Water-rock ratios (W/R) and reaction temperatures

Serpentinites from the basement rocks have Sr isotopic signatures close to seawater values (0.70885 to 0.70918;

Boschi et al., 2008; Delacour et al., 2008d), while gabbros from the southern wall of the Atlantis Massif have lower $^{87}Sr/^{86}Sr$ ratios between 0.70321 and 0.70642 (Delacour et al., 2008d) closer to that of unaltered mantle (0.70269; Workman & Hart, 2005). This indicates that serpentinization occurred at very high integrated water–rock ratios (W/R = 100 to 800; Boschi et al., 2008) but the hydrothermal fluids at the LCHF are still influenced by interaction with the variably altered mantle and/or gabbroic rocks at relatively lower water/rock ratios. Using our hydrothermal endmember $^{87}Sr/^{86}Sr$ ratio and Sr concentration and a protolith Sr content between 10 and 49 ppm (McDonough, 1990; Salters and Stracke, 2004), we estimate that the Lost City vent fluids have experienced W/R ≈ 3 to 13 (equation 11; Berndt et al., 1988). The use of a higher upper limit of 49 ppm for the average protolith Sr concentrations (McDonough, 1990) resulted to a higher upper limit for the calculated W/R ratios compared to the earlier calculations of Foustoukos et al. (2008). Using the mass-balance equation described by Taylor (1977), an initial fluid with $\delta^{18}O = 0$ (i.e., seawater), and olivine and serpentine $\delta^{18}O$ values reported in Rouméjon et al. (2018b), we obtain W/R ratios between 4 and 18. These W/R ratios are in strong agreement with those calculated from Sr geochemistry. In addition, using the temperature dependent serpentine-water oxygen isotope fractionation of Saccocia et al. (2009) and the serpentine $\delta^{18}O$ values reported in Rouméjon et al. (2018b), we estimate serpentinization reaction temperatures of ~ 300 °C. Using a very similar approach, Foustoukos et al. (2008) combined W/R ratios obtained from $^{87}Sr/^{86}Sr$ with previously reported $\delta^{18}O$ composition of the LCHF vent fluids (Kelley et al., 2005) and calculated reaction temperatures of ~ 300 °C. This relatively high reaction temperature for the LCHF basement rocks is supported by other estimates. These include $\delta^{18}O$ data from carbonate veins (up to 225 °C; Früh-Green et al., 2003) and serpentinites from the basement (210 to 450 °C; Rouméjon et al., 2018b), thermodynamic modelling of vent fluids (140–300 °C; Allen and Seyfried, 2004; Foustoukos et al., 2008; Lang et al., 2012; Seyfried et al., 2015), and more recently, thermometry based on clumped isotopes in methane (apparent $\Delta^{13}CH_3D$ temperatures between 158 and 270℃, Wang et al., 2018; Labidi et al., 2020). Finally, we compared our calculated in-situ pH and measured exit temperatures (Table 2) with the theoretical models of Foustoukos et al. (2008). Fig. 7 suggests that the fluids venting at Beehive can be consistent with the conductive cooling of a > 300 °C fluid at W/R > 1. Interestingly, the pH of the fluids venting from the other vents indicate higher W/R ratios relative to Beehive.

4.3. Sulfate reduction and addition of seawater sulfate

In the presence of electron donors (e.g., H_2, reduced C compounds), sulfate reduction can occur according to the following reaction (written with H_2):

$$SO_4^{2-} + 4H_2 \rightarrow HS^- + OH^- + 3H_2O. \quad (1)$$

At Lost City, endmember H_2S concentrations are lowest in the central vents and increase towards the peripheral high sulfide and eastern wall vents. In contrast, SO_4^{2-} and H_2 concentrations decrease towards the peripheral vents (Fig. 3). The overall change in the concentrations across vent sites roughly corresponds to those expected during sulfate reduction (Equation (1), Fig. 3). This pattern has been previously used to suggest that microbial sulfate reduction (MSR) is an important control on the LCHF vent fluid chemistry (Kelley et al., 2005; Proskurowski et al., 2006; Lang et al., 2012). The fluid $\delta^{34}S$ signatures, however, cannot be explained by a simple model that considers only sulfate reduction. With the exception of Beehive, all vent fluids have $\delta^{34}S_{sulfide}$ values that are higher than the correspond-

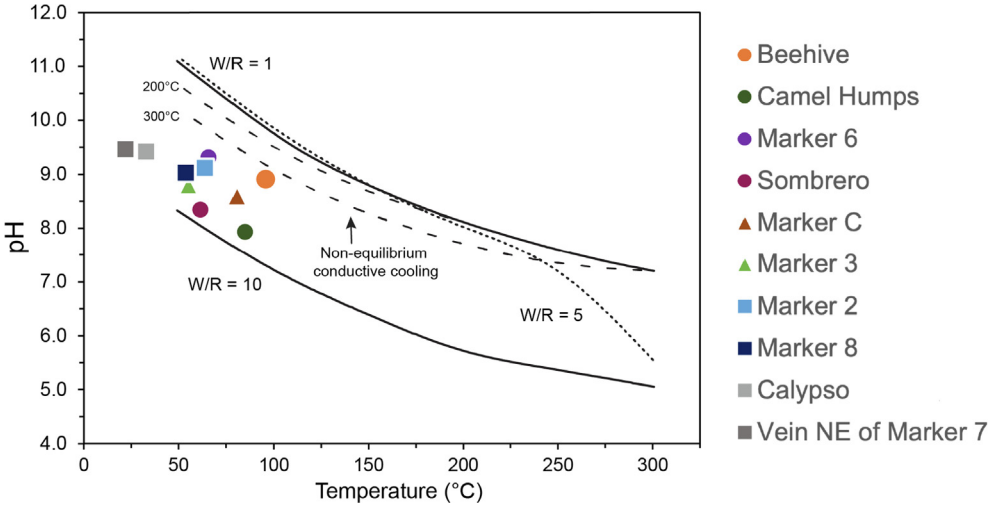

Fig. 7. Calculated in-situ pH vs. vent temperatures of the LCHF vent fluids plotted against theoretical models of Foustoukos et al. (2008). Shown are pH evolution pathways during peridotite-seawater equilibrium at 500 bars and temperatures between 50 and 300 °C at water/rock ratios (W/R) of 1, 5, and 10 (dotted and continuous lines). Dashed lines show the pH evolution during conductive cooling of seawater initially equilibrated with peridotite at W/R = 1 at 200 °C and 300 °C. The pH of fluids venting at Beehive can be consistent with conductive cooling of seawater equilibrated at > 300 °C and/or W/R > 1 while the pH of the other vents suggests higher W/R ratios.

ing $\delta^{34}S_{sulfate}$ (Table 2, Fig. 4C), whereas sulfate reduction, whether open-system or closed-system, produces sulfide that is depleted in ^{34}S relative to the reactant sulfate (Brunner and Bernasconi, 2005).

All hydrothermal fluids are predominantly derived from seawater (German and Von Damm, 2003), thus, comparison of observed isotopic signatures with those of seawater provides insights into the processes that produced these signatures. Both $\delta^{34}S_{sulfide}$ and $\delta^{34}S_{sulfate}$ in the LCHF vent fluids are higher than that of seawater sulfate (+21‰), which points to closed-system Rayleigh fractionation as the dominant process (Fig. 8). Unaltered peridotites have $\delta^{34}S_{sulfide}$ values of -0.7 ± 0.8‰ (bulk rock $\delta^{34}S$ values $= +0.3 \pm 0.5$‰; Sakai et al.,1984; Shanks et al, 1995); whereas hydrothermal sulfides originating by reaction with gabbroic intrusions have $\delta^{34}S$ values ranging from + 5 to + 10‰ (Alt et al., 2013). Hence, a contribution from these sources of sulfur cannot increase the LCHF vent fluid $\delta^{34}S$ to values higher than that of seawater sulfate. Allen and Seyfried (2004) and Lang et al. (2012) inferred that anhydrite solubility at 140 to 190 °C buffers the chemistry of the vent fluids at Lost City. However, the $\delta^{34}S$ data presented here is not consistent with the hypothesis that anhydrite solubility is the main or only control on the sulfur geochemistry of the vent fluids. Anhydrite precipitating upon heating of seawater to temperatures above ~ 150 °C (German and Von Damm, 2003) has $\delta^{34}S$ values slightly higher (+22 ± 0.7 ‰) but very close to seawater sulfate (Raab & Spiro, 1991; Kuhn et al., 2003). Thus, neither residual fluids after anhydrite precipitation nor contributions from anhydrite dissolution will significantly increase the $\delta^{34}S_{sulfate}$ in the vent fluids and will not produce ^{34}S-enriched sulfides. Closed-system reduction of sulfate with $\delta^{34}S = +21$‰ (i.e., seawater sulfate), on the other hand, can explain the $\delta^{34}S$ of sulfide and sulfate in the Beehive vent fluids. As sulfate reduction proceeds towards completion, the residual reactant sulfate and the instantaneous sulfide are progressively enriched in ^{34}S (Fig. 8). The reduction of sulfate to sulfide in a closed system will produce an increase in H_2S. The little to no H_2S contents of these fluids suggest that sulfide produced is removed in the subseafloor, likely due to precipitation as pyrite.

The associated equilibrium fractionation ($\varepsilon_{pyrite\text{-}H2S}$) during sulfide (pyrite) precipitation has been thought to be a small positive value (+0.8‰ at 150 °C; +0.1‰ at 200 °C (Kajiwara and Krouse, 1971; Ohmoto, 1972); +1.2‰ at 300 °C (Ohmoto and Rye, 1979)) although more recent experimental study suggests an $\varepsilon_{pyrite\text{-}H2S}$ value of the opposite direction (-1.9‰ at 350 °C; Syverson et al., 2015). Nevertheless, because of low equilibration rates typical of mid-ocean ridge hydrothermal systems, a disequilibrium, lower magnitude $\varepsilon_{pyrite\text{-}H2S}$ can be expected in natural samples (Syverson et al., 2015). In addition, $\varepsilon_{pyrite\text{-}H2S}$ approaches zero during almost complete precipitation from dissolved sulfide (see Sakai, 1968). Thus, it is possible for precipitated sulfide to record a similar $\delta^{34}S$ to that of the instantaneously produced dissolved sulfide.

The ^{34}S-enriched isotope signatures can be preserved in the vent fluids or in sulfide minerals that precipitate from these fluids during sulfate reduction provided that the reac-

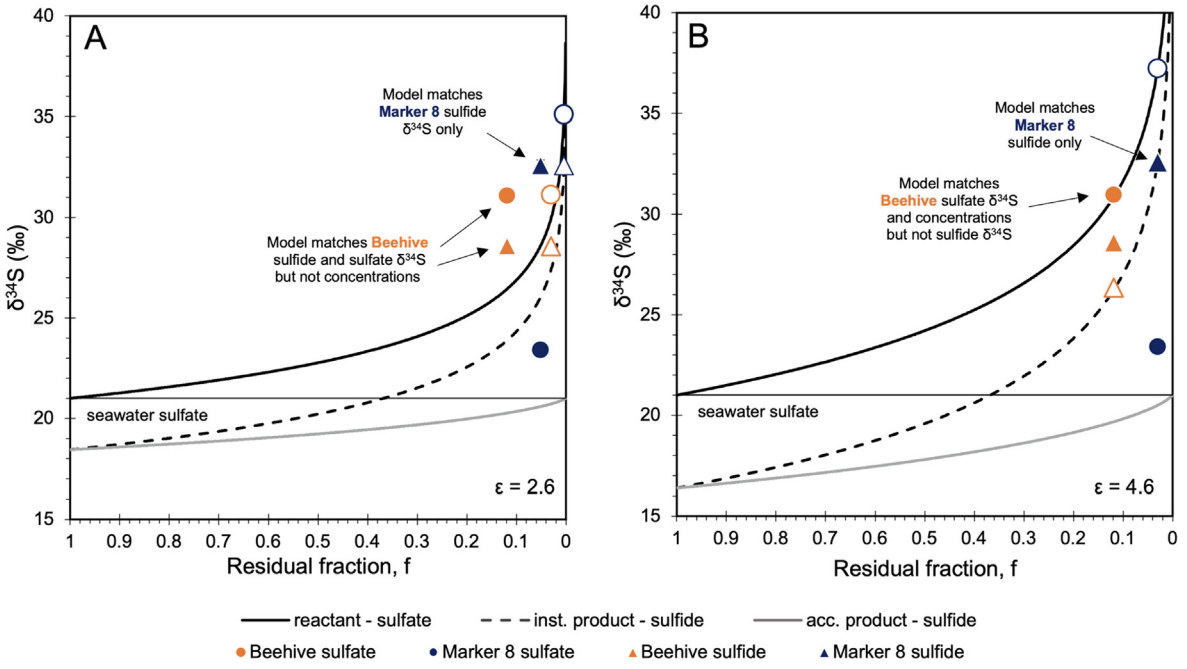

Fig. 8. Rayleigh fractionation modelling of Beehive and Marker 8 vent fluids using a fractionation factor ($\varepsilon_{sulfate\text{-}sulfide}$) of (A) 2.6 and (B) 4.6‰. (A) Beehive $\delta^{34}S$ values but not concentrations can be produced via closed-system sulfate reduction starting from a seawater-like fluid (28 mmol/kg sulfate, $\delta^{34}S_{sulfate} = +21$‰). Continued sulfate reduction can produce Marker 8 $\delta^{34}S_{sulfide}$ but not $\delta^{34}S_{sulfate}$. (B) Sulfate reduction with a slightly higher $\varepsilon_{sulfate\text{-}sulfide}$ value can produce sulfate with $\delta^{34}S$ and concentrations that match those observed at Beehive. Note: inst = instantaneous, acc – accumulated; filled symbols = measured endmember values, open symbols = model values that do not match with the measured values. Uncertainties are smaller than the symbol sizes.

tion zone is a nearly closed system with respect to sulfate. We hypothesize that anhydrite dissolution during cooling can provide dissolved sulfate with seawater-like $\delta^{34}S$ (Raab & Spiro, 1991; Kuhn et al., 2003) while maintaining generally closed-system conditions. Sulfate reduction is then followed by rapid and quantitative removal of instantaneously formed dissolved sulfide through precipitation of metal sulfides. Accumulated product sulfide formed during closed-system sulfate reduction has $\delta^{34}S$ values that do not exceed the reactant seawater sulfate (Fig. 8). Closed-system sulfate reduction may occur either in the shallower subsurface or in the deeper basement rocks. Evidence for closed-system sulfate reduction in the subsurface is supported by the presence of ^{34}S-enriched sulfide in the serpentinized peridotites from the southern wall of the Atlantis Massif (Delacour et al., 2008b; Liebmann et al., 2018). Closed-system MSR was also invoked to explain two serpentinite samples from the Iberian Margin which have $\delta^{34}S_{sulfide}$ values exceeding that of seawater (Alt and Shanks, 1998), suggesting that this process is not uncommon. More recently, Liebmann et al. (2018) attributed all $\delta^{34}S_{sulfide} > 0‰$ in the Atlantis Massif serpentinites to thermochemical sulfate reduction (TSR) and hydrothermal sulfide addition due to heating of entrained seawater at temperatures > 200 °C, which is more consistent with the metamorphic evolution of the Atlantis Massif (e.g., Boschi et al., 2006; Rouméjon et al., 2018a, 2018b).

4.3.1. Microbial versus thermochemical sulfate reduction

In Fig. 8, we use a Rayleigh distillation model to investigate the evolution of the $\delta^{34}S$ of the reactant sulfate, instantaneous sulfide, and accumulated sulfide during closed-system reduction of sulfate with $\delta^{34}S$ of + 21‰. A fractionation factor ($\varepsilon_{sulfate\text{-}sulfide}$) of 2.6‰ can produce the $\delta^{34}S$ values for sulfide and sulfate in the Beehive vent and the $\delta^{34}S_{sulfide}$ value for Marker 8 (Fig. 8A). Assuming an initial SO_4^{2-} of 28 mmol/kg (i.e., seawater), a $\varepsilon_{sulfate\text{-}sulfide}$ value of 4.6‰ can explain the sulfate $\delta^{34}S$ and concentrations in Beehive (Fig. 8B). It is, however, not possible to find a single $\varepsilon_{sulfate\text{-}sulfide}$ value that simultaneously reproduces the $\delta^{34}S$ of sulfide and sulfate, and sulfate concentrations observed in Beehive. Additional sources of ^{34}S-enriched sulfide, an initial SO_4^{2-} concentration greater than 28 mmol/kg, and/or a non-constant $\varepsilon_{sulfate\text{-}sulfide}$ and $\varepsilon_{pyrite\text{-}H2S}$ (e.g., Ohmoto, 1972; Sakai, 1968; Syverson et al., 2015) values over time may explain this discrepancy. Moreover, the vent fluid dissolved sulfide concentrations do not necessarily represent the instantaneous product sulfide at the corresponding sulfate concentration (or residual fraction) but reflects multiple processes over the residence time of the fluids. Overall, $\varepsilon_{sulfate\text{-}sulfide}$ values between ~ 3 and 5‰ can explain the sulfur geochemistry of the Beehive vent fluid.

Sulfur isotope fractionations associated with MSR span a wide range and depend on many factors such as bacteria strain, availability of electron donors, growth rates, temperature, and pH (e.g. Detmers et al., 2001; Kemp & Thode, 1968; Sim et al., 2011, Brunner & Bernasconi 2005). While MSR typically leads to depletion in ^{34}S in the product sulfide with large fractionations of up to 75‰ (Brunner & Bernasconi 2005), relatively low sulfur isotope fractionation has been reported for culture experiments using H_2 as an electron donor at temperatures from < 35 °C to 80 °C (1 to 9.7‰; Kemp & Thode, 1968; Hoek et al., 2006). Unfortunately, culture experiments conducted at the relatively higher temperature and higher pH conditions (e.g. temperatures > 90 °C, pH > 9) characteristic of Beehive are unavailable. While MSR cannot be excluded as the source of the observed small fractionation, an alternative is that it is produced by thermochemical sulfate reduction. The isotope fractionation during TSR is about 20‰ at ~ 100 °C and decreases to about 5‰ at 350 °C (Kiyosu and Krouse, 1990). TSR is thought to involve the reduction of SO_4^{2-} with organic compounds and, to our knowledge, experiments on TSR using H_2 are currently unavailable. Experiments involving organic compounds suggest that isotopic fractionation is generally independent of the electron donor involved (Kiyosu and Krouse, 1990). Overall, the fractionation factor observed in Beehive can be reconciled with either microbial or thermochemical sulfate reduction at high temperatures.

Temperature is likely the key control on whether the sulfate reduction process that produced the Beehive vent fluids occurred via MSR or TSR. MSR is the dominant process at temperatures below ~ 80 °C (Postgate, 1984) and have been reported to occur at temperatures of up to 110 °C in deep-sea hydrothermal vent sediments (Jørgensen et al., 1992; Elsgaard et al., 1994). On the other hand, TSR is possible only at temperatures exceeding ~ 80–100 °C (Worden et al., 1995; Machel et al., 1995; Machel 1998; 2001) and is thought to be significant in hydrothermal systems at temperatures above 200 °C (Mottl et al., 1979; Ohmoto and Lasaga, 1982). The temperatures observed at Beehive (up to ~ 100 °C) are close to the temperature divide between MSR and TSR. However, multiple lines of evidence point to temperatures well above the range for MSR in the LCHF subsurface (see section 4.2). If the high $\delta^{34}S$ signatures in the Beehive fluids are produced at depth, sulfate reduction at higher temperatures via TSR is a more plausible explanation. This interpretation is consistent with the generally high $\delta^{34}S$ values in the vent fluids, since the deeper and likely less altered basement rocks are more representative of a closed system than the shallower serpentinites or the porous chimney interiors. As discussed above, ^{34}S-enriched sulfides were also found in the serpentinites from the Atlantis Massif, and their origin was attributed to closed system-thermochemical sulfate reduction (Delacour et al., 2008b; Liebmann et al., 2018).

4.3.2. Controls on S chemistry and isotopic compositions

With the exception of Beehive, the $\delta^{34}S$ of dissolved sulfate in the vents is significantly lower than that of the coexisting sulfide (Table 2, Fig. 4C). Closed-system sulfate reduction alone cannot explain the sulfur isotope data, because although it produces sulfide and sulfate isotopically heavier than the initial seawater sulfate, the $\delta^{34}S$ of sulfate should be higher than that of sulfide. Fig. 8 shows that closed-system sulfate reduction of a fluid with seawater $\delta^{34}S$ can produce isotopically heavy sulfides characteristic of both Beehive and Marker 8. The variability in $\delta^{34}S_{sulfide}$

in the Lost City fluids can be explained by the addition of variable amounts of ^{34}S-enriched sulfide produced from the residual sulfate, with the Beehive and Marker 8 vents representing the lowest and highest extents of reaction, respectively. This can be achieved if the vents with the higher $\delta^{34}S_{sulfide}$ values have a longer flow path or a slower fluid flow than Beehive at depth, allowing protracted sulfate reduction under closed-system conditions. However, more extensive sulfate reduction would also produce higher $\delta^{34}S_{sulfate}$ values in the vents, which is not the case (Figs. 4C, 8). This requires addition of isotopically lighter sulfate in some of the vents or the precipitation of isotopically lighter sulfide minerals. Precipitation of ^{34}S depleted sulfide minerals, however, should result in lower dissolved sulfide concentrations in the vents with higher $\delta^{34}S_{sulfide}$ values. We observe that $\delta^{34}S_{sulfide}$ values generally increase with increasing H_2S concentrations (Fig. 9A). Moreover, precipitation of sulfide minerals does not explain the $\delta^{34}S_{sulfate}$ values approaching seawater sulfate in the lower temperature vents (Fig. 9B). Thus, we suggest that addition of ^{34}S-depleted sulfate, for example, from seawater infiltration or anhydrite dissolution, in some of the vents can explain the $\delta^{34}S_{sulfide} > \delta^{34}S_{sulfate}$ values.

Assuming that the rest of the vents are formed from Beehive, Marker C, and Marker 2, respectively (Fig. 6), we can evaluate the processes that control the variations in sulfur chemistry and isotopes by comparing the endmember composition of each vent with the highest temperature vent within each group (Fig. 9). For example, the low sulfide vents show an increase in $\delta^{34}S_{sulfide}$ at Sombrero relative to Beehive and Camel Humps which can be produced by a longer extent of sulfate reduction, while a decrease in $\delta^{34}S_{sulfate}$ would indicate a contribution of fresh seawater sulfate or anhydrite dissolution. Camel Humps has the same $\delta^{34}S_{sulfide}$ but lower sulfate concentrations and $\delta^{34}S_{sulfate}$ than Beehive, suggesting consumption via active sulfate reduction fueled by sulfate replenishment (Fig. 9B). Marker 3 and Marker C (moderate sulfide group) have higher H_2S concentrations and $\delta^{34}S_{sulfide}$ than the low sulfide group, which may be formed from a protracted closed-system sulfate reduction (Fig. 9A). Marker 3 has lower $\delta^{34}S_{sulfide}$ than Marker C, despite its lower temperature and slightly higher dissolved H_2S concentrations. The reaction rates for thermochemical sulfate reduction at these relatively low temperatures are geochemically insignificant (Kiyosu, 1980; Ohmoto and Lasaga, 1982). Thus, an addition of ^{34}S-depleted H_2S to the Marker 3 vent fluid, likely from open-system microbial seawater sulfate reduction, can explain this. This complements the slight increase in SO_4^{2-} concentration and decrease in $\delta^{34}S_{sulfate}$ (Fig. 9B) at Marker 3, which indicates incorporation of seawater sulfate or anhydrite dissolution in an open system. Both open- and closed-system sulfate reduction, as well as incorporation of seawater sulfate are also recorded in the serpentinites from the Atlantis Massif and support our interpretations (Delacour et al., 2008b; Liebmann et al., 2018). The $\delta^{34}S_{sulfate}$ values of the moderate sulfide group are significantly lower than Beehive and comparable to those of

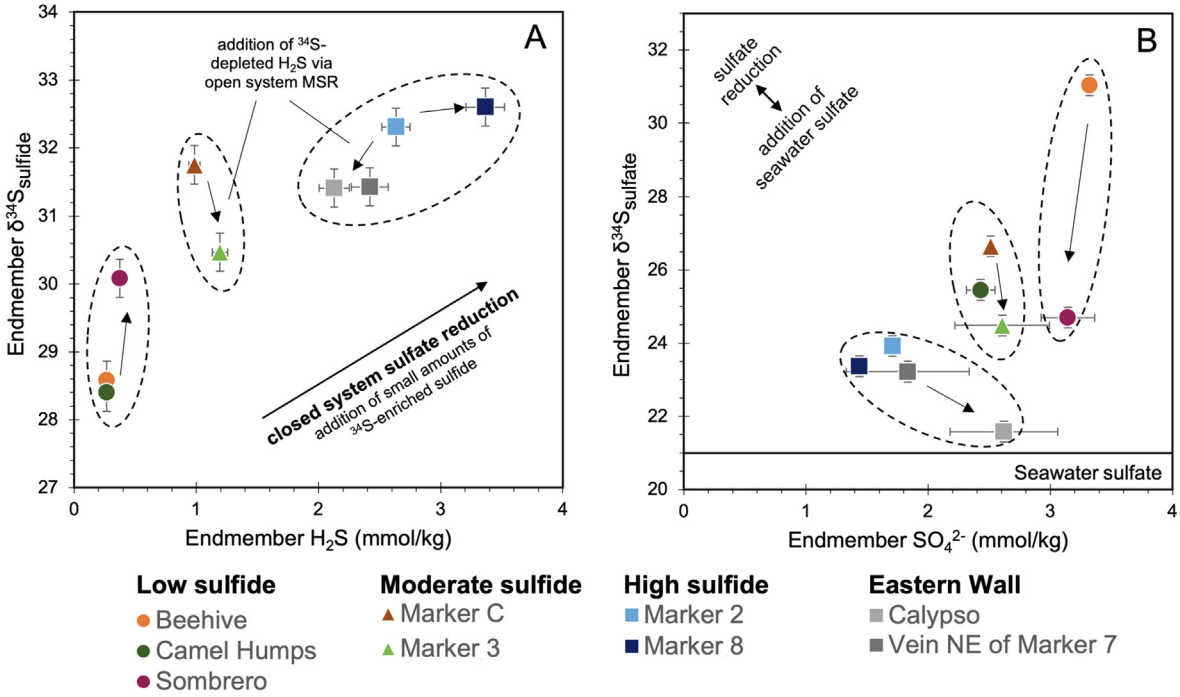

Fig. 9. Endmember sulfur concentrations and isotope compositions of the LCHF vent fluids. Variations reflect multiple processes that control these compositions across the field. (A) Endmember H_2S and $\delta^{34}S_{sulfide}$ broadly reflect addition of ^{34}S-enriched H_2S from closed-system sulfate reduction. Marker 3 and the eastern wall vents are an exception and reflect addition of ^{34}S-depleted H_2S likely from open-system microbial sulfate reduction. (B) Endmember SO_4^{2-} and $\delta^{34}S_{sulfate}$ compositions suggest integrated effects of sulfate reduction and addition of seawater sulfate. Arrows show general direction of these two processes.

Camel Humps and Sombrero, implying an addition of ^{34}S-depleted sulfate (Fig. 9B). The highest $\delta^{34}S_{sulfide}$ and H_2S and lowest SO_4^{2-} concentrations of the high sulfide group (Markers 2 and 8) indicate that they have experienced the most extensive closed-system sulfate reduction (Fig. 9). Lower $\delta^{34}S_{sulfide}$ and H_2S concentrations in the eastern wall vents points to a lower extent of sulfate reduction than the high sulfide vents (Fig. 9A). Calypso and the vein NE of Marker 7, sites that are furthest from the Poseidon structure (Fig. 1) and have the lowest venting temperatures, also have $\delta^{34}S_{sulfate}$ values closer to seawater (Table 2, Fig. 9B) reflecting a significant influence of seawater sulfate.

4.4. Methane and hydrogen geochemistry

Measured H_2 and CH_4 plotted against measured Mg concentrations for both the 2018 and 2003 data (Proskurowski et al., 2006) are shown in Fig. 10 and listed in Table 3. Mixing lines between endmember compositions of several high-temperature vents (Beehive, Marker C, Marker 2, Marker 6) with seawater are also shown. Despite having the highest venting temperature, Beehive does not have the highest endmember H_2 and CH_4 concentrations, which are observed at Marker 6. In addition, mixing between seawater and Marker 6 endmember fluids, instead of Beehive, can account for the measured H_2 and CH_4 concentrations of the low sulfide vents (Fig. 10A, D). The high H_2 and CH_4 concentrations observed at Marker 6 may potentially be explained by its proximity to the serpentinite basement where these volatiles are thought to be sourced (Proskurowski et al., 2006; Wang et al., 2018; Labidi et al., 2020). In contrast, Beehive is located high up on the 60-m carbonate structure Poseidon and not directly on the basement rocks (Fig. 1C). Nevertheless, a strong correlation between measured H_2 and CH_4 concentrations of the low sulfide vents, including both Beehive and Marker 6 (Fig. 10G), suggest a common flow path for this group. Although there is some scatter in some of the vents, measured H_2 and CH_4 concentrations in the moderate sulfide and high sulfide groups (Fig. 10B-C, E-G) reflect mixing between seawater and either Marker C or Marker 2 endmember fluids, as is also observed from the sulfur chemistry (Figs. 2, 6).

Endmember H_2 concentrations defined for each vent group show a decreasing trend from the central low sulfide vents towards the more peripheral high sulfide vents, while the endmember CH_4 calculated from all the vent groups (with the exception of the Marker 6 mixing line) are within a narrow range of 1.1 ± 0.1 to 1.2 ± 0.1 mmol/kg (Fig. 10, Table 3). The origin of volatiles at the LCHF has been discussed elsewhere (Proskurowski et al., 2006; Proskurowski et al., 2008; Bradley and Summons, 2010; Wang et al., 2018; Labidi et al., 2020). Nevertheless, this observation is consistent with recent findings that CH_4 in hydrothermal systems, independent of basement rock type and/or venting temperatures, are formed abiotically at greater depths and temperatures (~400℃), and may be stored in olivine-hosted fluid inclusions over geological time scales prior to venting (Kelley and Früh-Green, 1999; Kelley and Früh-Green, 2001; McDermott et al., 2015; Wang et al., 2018; Klein et al., 2019; Labidi et al., 2020).

4.5. Multi-stage evolution of the LCHF fluids

The Sr isotope compositions of the LCHF fluids clearly suggest that all the vent fluids investigated are derived from a single primary endmember (Fig. 5). However, the sulfur and hydrogen geochemistry suggests a more complex evolution with compositions that roughly reflect temperature and/or location. We propose a conceptual model (Fig. 11) that integrates processes in the basement and in the shallower subsurface which reflect a transition from a dominantly closed to a dominantly open system with increasing seawater influence.

4.5.1. First-order vent

Beehive, located at the center of the main vent field, discharges the hottest (96 °C) fluids and can be considered the first-order endmember fluid (Fig. 11A). Unlike the rest of the vents, $\delta^{34}S_{sulfate}$ is higher than $\delta^{34}S_{sulfide}$ at Beehive, a relative magnitude consistent with sulfate reduction. As this fluid is predominantly derived from seawater, direct comparison of its composition with that of seawater gives us information on seawater-rock interactions in the basement and/or within the hydrothermal structures along the flow path. Seawater Mg is removed through Mg mineral precipitation (e.g., serpentine and/or brucite), resulting in a zero Mg composition (Allen and Seyfried, 2004; Foustoukos et al., 2008; Seyfried et al., 2015). Beehive vent fluids contain 3.3 mmol/kg SO_4^{2-} and 0.3 mmol/kg H_2S with distinctly higher $\delta^{34}S$ than seawater. As seawater is heated to temperatures > 150℃, at least 25 mmol/kg of sulfate is removed, most likely through anhydrite precipitation (Sleep, 1991; Shanks, 2001) and incorporation into the serpentinites during water–rock reactions in the basement (Delacour et al., 2008b). Cooling to temperatures < 150℃ in a generally closed system results in the dissolution of anhydrite, thermochemical sulfate reduction (see Section 4.3) of sulfate sourced from dissolution of anhydrite, and subsequent removal by sulfide precipitation. Dissolved sulfide in the Beehive vent fluids is formed during sulfate reduction and probably from the dissolution of earlier formed sulfide minerals, consistent with the observed depletion of sulfide-sulfur in the rocks from the southern wall of the Atlantis massif, which was attributed to the removal of sulfide-sulfur by circulating seawater over long time scales (Delacour et al., 2008b).

4.5.2. Second-order vents

Marker C and Marker 2 are the high temperature endmembers of the other two mixing lines defined by sulfur and volatile chemistry (Figs. 6, 10, 11B). The 80 °C Marker C vent is located in the center of the field adjacent to Beehive while Marker 2, which vents 62 °C fluids, is located in the western part of the main field. Both vents have close to zero Mg concentrations and have the highest $\delta^{34}S_{sulfate}$ within their group (Table 2, Fig. 9B). The $\delta^{34}S_{sulfide}$ values are higher than in Beehive and $\delta^{34}S_{sulfate}$ are lower, progressively approaching seawater sulfate values (Fig. 9). These second-order vents cannot be simple mixtures of seawater and Beehive endmember fluid. We hypothesize that the endmember fluids rise through the basement and migrate later-

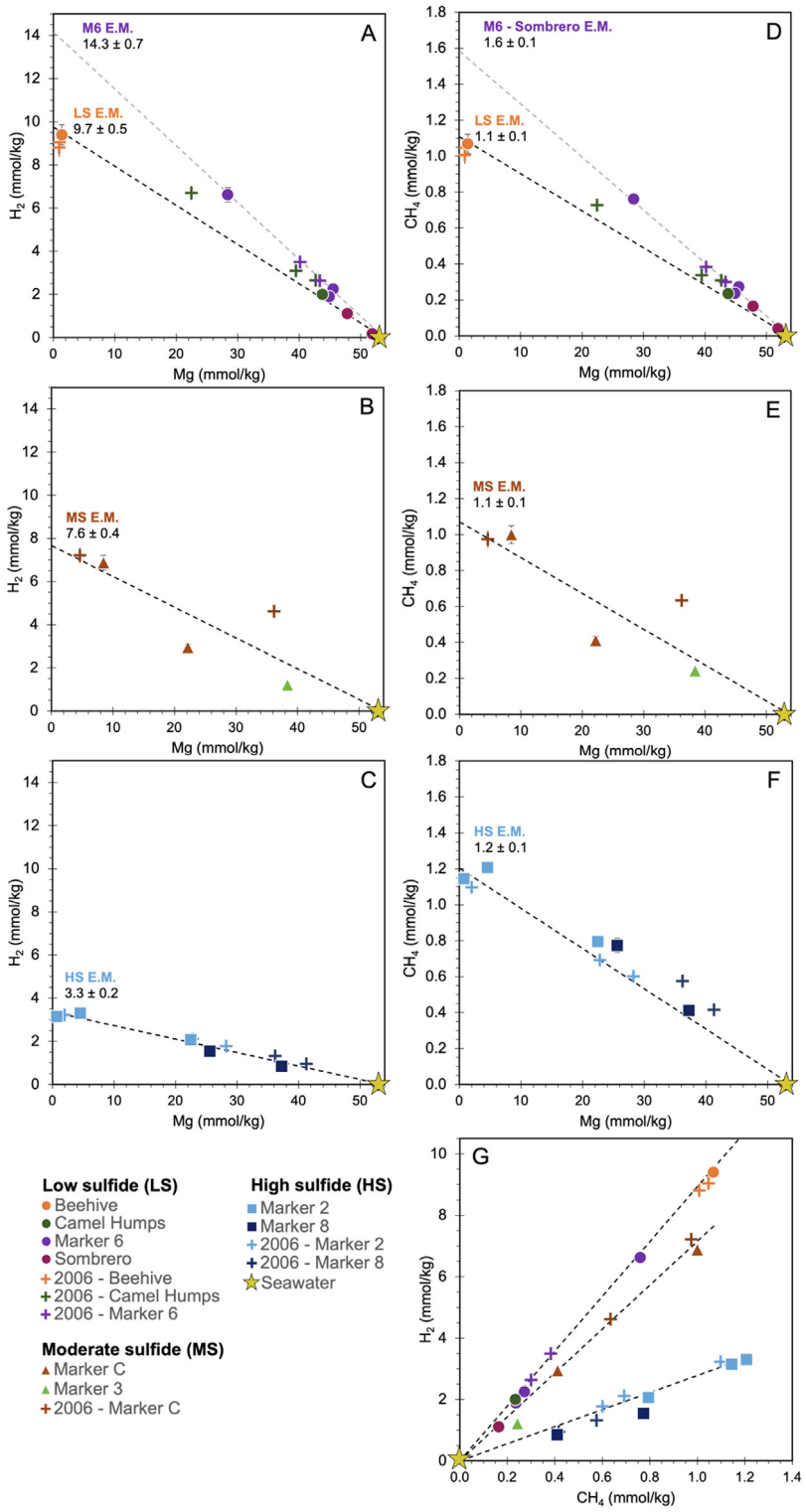

Fig. 10. Measured and endmember volatile compositions at LCHF. (A-C) Measured H_2 concentrations plotted against measured Mg define three separate mixing lines for each of the vent group (low, moderate, and high sulfide groups). This suggests that there are at least three endmember H_2 compositions at LCHF. (D-F) Measured CH_4 concentrations against Mg for each of the vent groups. Except for those calculated from the Marker 6 mixing line, endmember CH_4 compositions are within a narrow range between 1.1 and 1.2 mmol/kg. Unlike those defined by sulfur chemistry (Fig. 6), mixing between seawater and Marker 6, instead of Beehive, can explain the volatile composition of the low sulfide vent group. (G) Measured H_2 and CH_4 concentrations are strongly correlated within each vent group suggesting a common flow path for each group. Symbols indicated as crosses (+) are data from Proskurowski et al. (2006). $^{87}Sr/^{86}Sr$ data are not available for all samples, thus, measured concentrations are plotted against Mg.

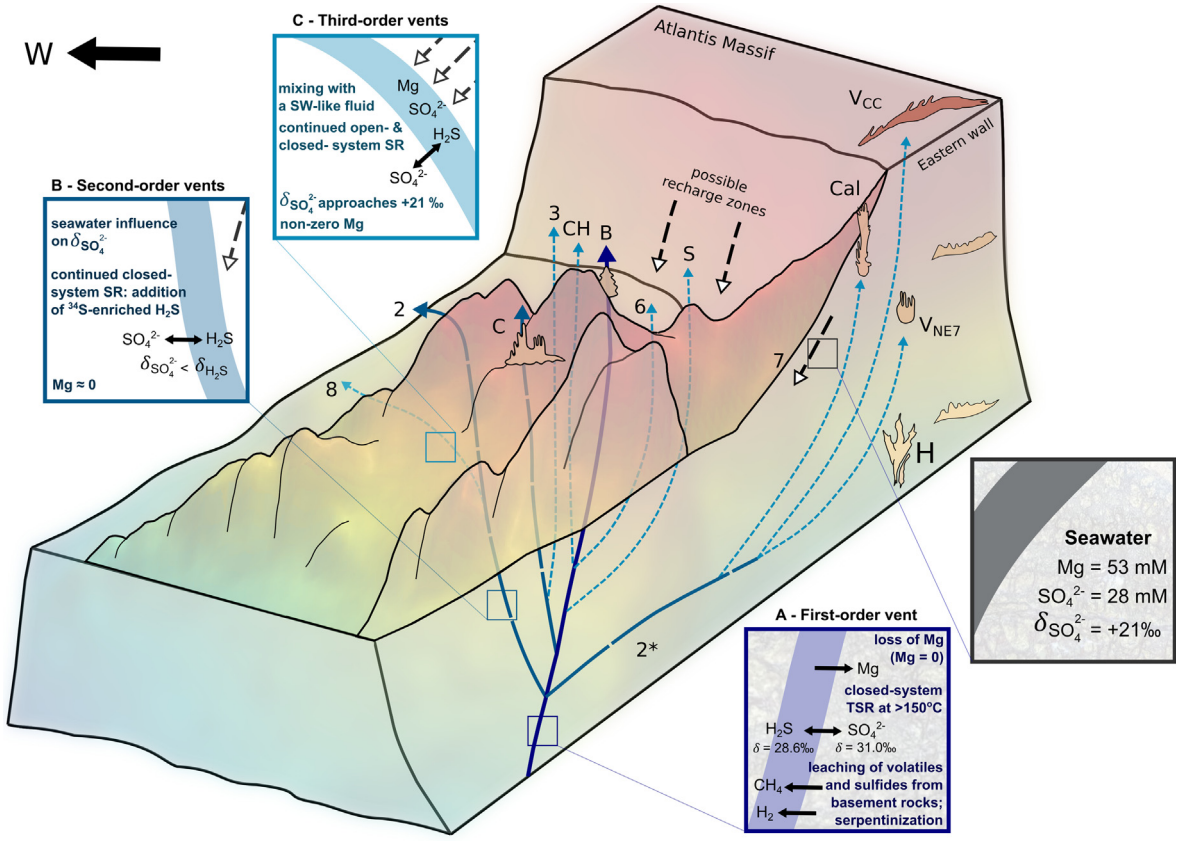

Fig. 11. Schematic diagram showing the spatial and compositional relationship among the LCHF vents based primarily on sulfur chemistry and sulfur isotopic compositions. (A) We suggest that all LCHF vent fluids originate from a single first-order (primary) endmember with a composition close to that of the Beehive vent. The composition of this primary vent fluid is a result of a combination of processes including high temperature (at least 70°C) removal of Mg, closed-system thermochemical sulfate reduction (TSR) of seawater (SW) sulfate and subsequent sulfide mineral precipitation, and leaching of volatiles produced by ongoing serpentinization reactions or released from olivine-hosted fluid inclusions in the basement rocks. At Beehive, sulfate reduction (SR) produces $\delta^{34}S_{sulfate} > \delta^{34}S_{sulfide}$. (B) Continued SR of the first order-fluid in a partially closed system results in the addition of ^{34}S-enriched H_2S in the second-order vents, Marker C and Marker 2. An influx of seawater results in $\delta^{34}S_{sulfate}$ lower than those observed in Beehive and $\delta^{34}S_{sulfate} < \delta^{34}S_{sulfide}$, the inverse of what is expected from SR. (C) Third-order vents are formed from subsurface mixing between the first- and second-order vent fluids with a SW-like fluid. $\delta^{34}S_{sulfide}$ is affected by both open- and closed-system SR, which can be microbial in these low temperature vents, while $\delta^{34}S_{sulfate}$ progressively approaches seawater values (+21‰) as temperature decreases. Notes and abbreviations: black arrows – seawater; dark blue arrows – first-order vent (B = Beehive); blue, coarsely-dashed arrows – second order vents (Markers 2 & C); light blue, finely-dashed arrows – third-order vents (CH = Camel humps, S = Sombrero, Cal = Calypso, V_{cc} = Vein on carbonate cap, V_{NE7} = vein northeast of Marker 7). Numbers refer to field marker numbers; 2* = hypothetical vent with compositions similar to Marker 2 that likely serves as a second-order vent for the eastern wall vents. See Fig. 1 for vent locations and Section 2.1 for explanation of vent names. (For interpretation of the references to colour in this figure legend, the reader is referred to the web version of this article.)

ally in a still partially closed system, via diffuse flow or fractures, and are then focused to produce the vents. Flow paths for Marker 2 are either longer or have a slower flow compared to those of Marker C, allowing Marker 2 vent fluids to experience, or to leach rocks that have experienced, more extensive closed-system sulfate reduction. The different flow paths of the second-order vents result in the addition of progressively isotopically enriched $S_{sulfide}$. At the same time, with increasing distance from the primary fluid conduit and W/R ratios (Figs. 7, 9), these second-order vents incorporate SO_4^{2-} with $\delta^{34}S$ close to + 21‰, either through admixture of seawater or via anhydrite dissolution. Despite the addition of seawater sulfate, continued sulfate reduction, likely mediated by microbial activity at these lower temperatures, leads to an overall decrease in SO_4^{2-} concentrations in the second-order vents (Fig. 9B).

4.5.3. Third-order vents

The third-order vents are formed from subseafloor mixing between the first- and second-order vents with seawater (Figs. 6, 10, 11C). The sulfur geochemistry of these vents reflects an influence of multiple processes including addition of seawater sulfate and H_2S from both open- and closed-system sulfate reduction. (Figs. 6, 9, see Section 4.3.2). The third-order vents are characterized by variable non-zero Mg endmember concentrations (Table 2). This is consistent with the calculations of Lowell (2017) indicating high Mg concentrations at Marker 3 relative to

the observed temperature, which was attributed to local entrainment of seawater. Mg is also possibly added via dissolution of brucite during mixing of relatively low pH seawater as the system transitions to open-system conditions (Templeton and Ellison, 2020; Klein et al., 2020). To date, no petrological studies have found brucite in the basement rocks of LCHF (Früh-Green et al., 2018). The thermodynamic models of Allen & Seyfried (2004) and Foustoukos et al. (2008) predicted brucite to be part of the equilibrium mineral assemblage at the basement of Lost City, while a more recent work (Seyfried et al., 2015) suggested that brucite is unstable. Even if brucite is currently precipitating at the basement rocks of Lost City, a combination of higher W/R, lower temperatures, and increasingly open-system conditions in the third-order vents (Fig. 9) will render brucite unstable allowing for its dissolution (Templeton and Ellison, 2020; Klein et al., 2020).

Within the low sulfide group (Figs. 6, 10A, D), the third-order vents include Camel Humps, Sombrero, and possibly, Marker 6. There is, however, a possibility that Marker 6 is a second-order vent because of its relatively high temperature (66 °C, Table 2) and H_2S concentrations (Fig. 6) and its highest dissolved volatile concentrations (Fig. 10A, D). Nevertheless, this confirms the work of Seyfried et al. (2015) suggesting a common source fluid for Beehive and Marker 6. Marker 3 represents the third-order vent for the moderate sulfide mixing line. The third-order vents in the high sulfide and eastern wall group include Marker 8, Calypso, Marker H (sampled only in 2003) and the carbonate veins (Figs. 6, 11B, C), all of which are located at the periphery of the field. We hypothesize that the eastern wall vents are likely derived from fluids similar to Marker 2.

5. CONCLUSIONS

Hydrogen concentrations of the LCHF vents vary systematically with SO_4^{2-} and H_2S concentrations, as well as $\delta^{34}S_{sulfide}$ (Figs. 4, 9A), pointing to sulfate reduction as a major control on the vent fluid compositions. The vents can be subdivided into four groups reflecting systematic variations in H_2 and S chemistry, temperature, and location within the field. Three groups are located in the main vent field on the Poseidon structure: the (1) low sulfide vents, the (2) moderate sulfide vents, and the (3) high sulfide vents. The fourth group (4), the eastern wall vents, is located along a steep northeast-southwest trending wall northeast of the main vent field. $^{87}Sr/^{86}Sr$ ratios of the fluids show that all vents were formed from the modification of a single endmember fluid with a composition close to that of the Beehive vent. This first-order vent fluid has nearly zero magnesium, $\delta^{34}S_{sulfide} < \delta^{34}S_{sulfate}$, and has lost at least 25 mmol/kg of sulfate through anhydrite precipitation and incorporation into the serpentinites. Subsequent cooling results to the dissolution of anhydrite followed by thermochemical sulfate reduction. The initial stages of water–rock interaction take place in a dominantly closed system at a relatively higher temperature allowing closed-system thermochemical sulfate reduction to occur. The rest of the vents are influenced by additional processes. Addition of sulfate via infiltration of seawater or anhydrite dissolution coupled with continued sulfate reduction result in the formation of second-order vents. These fluids are modified in an increasingly open system, where they experience incorporation of seawater sulfate, open-system microbial sulfate reduction, and possibly addition of Mg, to produce third-order vents. CH_4 concentrations are constant across the field, which suggests an origin independent of vent temperatures and circulation and which is consistent with methane being of deep origin (Kelley & Früh-Green, 1999; 2001; Wang et al., 2018; Klein et al., 2019; Labidi et al., 2020).

Our results highlight that the composition of the primary endmember vent fluid at LCHF is produced in the absence of microbial activity in the deeper, hotter serpentinite subsurface in a dominantly closed system. The microbial communities in the chimneys and vent fluids of LCHF (Schrenk et al., 2004; Brazelton et al., 2006) likely thrive in an environment characterized by substantial mixing of seawater with hydrothermal fluids (c.f., Amend et al., 2011; Lang & Brazelton 2020).

DECLARATION OF COMPETING INTEREST

The authors declare that they have no known competing financial interests or personal relationships that could have appeared to influence the work reported in this paper.

ACKNOWLEDGEMENTS

We thank the captain and crew of the R/V Atlantis, ROV Jason, and the scientific party of the 2018 expedition AT42-01. Funding was provided by NSF awards OCE- 1536702 / 1536405 / 1535962, the Swiss National Science Foundation project No. 200021_163187, the Joint Institute for the Study of the Atmosphere and Ocean (JISAO) under NOAA Cooperative Agreement NA15OAR4320063 - Contribution No. 2021-1132, the Deep Carbon Observatory, and the Philippine Department of Science and Technology–Science Education Institute (DOST-SEI). The authors also thank Tamara Baumberger for help at sea with the gas samples, Madalina Jaggi for generous assistance during the stable isotope analyses, Eric Olson for the gas concentration analyses, Kevin Roe for major element analyses at PMEL, and Reto Wijker for sulfate analyses at ETH Zurich. We thank the associate editor, an anonymous reviewer, and Eoghan Reeves for constructive comments that greatly improved our manuscript. This publication is PMEL contribution number 5236.

APPENDIX A. CALCULATION OF ENDMEMBER COMPOSITIONS

Pure hydrothermal vent fluids in high temperature (>300 °C) black smoker systems typically contain close to 0 mmol/kg Mg, while average background seawater contains about 53 mmol/kg Mg (Bischoff & Dickson, 1975; Mottl & Holland, 1978). During sampling of hydrothermal vents, background seawater is inevitably entrained with the hydrothermal fluids. Thus, measured compositions have to be corrected for seawater entrainment during sampling. This is conventionally done by plotting the measured compositions versus Mg and obtaining the composition where the regression line intercepts Mg = 0 (e.g. Von Damm et al., 1985). However, unlike in high temperature black

smoker systems where Mg is quantitively removed by basalt-water interaction (Bischoff & Dickson, 1975; Mottl & Holland, 1978), the removal of Mg at lower temperature hydrothermal systems (<65 °C) is incomplete and varies with temperature (see Fig. 2B in Shalev et al., 2019). This is important because some of the structures at Lost City emit fluids with temperatures less than < 65 °C (Table 2). If not all vent fluids have zero Mg compositions, either because it is not fully removed or because it is reintroduced during lower temperature circulation through the system, calculation of endmember compositions by extrapolation to a zero Mg endmember may overestimate the amount of seawater entrained during sampling and lead to inaccurate correction of the vent fluid compositions.

In the following, we evaluate the application of radiogenic strontium isotope compositions as an alternative method for calculating endmember vent fluid compositions. In hydrothermal systems, endmember Sr isotope compositions are obtained by plotting measured $^{87}Sr/^{86}Sr$ values against Mg/Sr, and determining the $^{87}Sr/^{86}Sr$ ratio at Mg/Sr = 0 (e.g., Albarède et al., 1981; Ludwig et al., 2006; Fig. 5). Fig. 5 suggests a two-component mixing between seawater with a $^{87}Sr/^{86}Sr$ ratio of 0.70917 ± 0.00001 (Palmer and Edmond, 1989) and a vent fluid endmember with a $^{87}Sr/^{86}Sr$ ratio of 0.70650 ± 0.00001, consistent with previous studies of Ludwig et al. (2006). Although several vents appear to have measured compositions that do not plot along the seawater-hydrothermal endmember mixing line, this can be best explained by the addition of Mg possibly via dissolution of brucite or seawater entrainment (Sections 4.1 and 4.5.3). Carbonates from Lost City chimneys have $^{87}Sr/^{86}Sr$ ratios higher than 0.70650 (0.70760–0.70913; Ludwig et al., 2006), thus, dissolution of carbonate chimneys will bring the data points above the mixing line. Anhydrite precipitation occurs at temperatures above 150 °C (German and Von Damm, 2003) and cannot occur at the temperatures of mixing between seawater and hydrothermal fluids (i.e., < 116 °C). Sr released during anhydrite or carbonate dissolution, will decrease the measured Mg/Sr, and cannot be used to explain the observed small deviations from the mixing line. Conversely, Sr incorporation during carbonate precipitation will increase the Mg/Sr of the fluids without affecting the $^{87}Sr/^{86}Sr$ ratios (Coggon and Teagle, 2011). However, since the deviation from the mixing line can be seen both in the $^{87}Sr/^{86}Sr$ vs. Mg and $^{87}Sr/^{86}Sr$ vs. Mg/Sr plots (Fig. 5) we can conclude that addition of Mg and not loss/gain of Sr can explain this deviation. In addition, measured SO_4^{2-} and Mg concentrations for some of the lower temperature vents plot in a mixing line between seawater and a zero-sulfate and zero-Mg endmember even though $\delta^{34}S_{sulfate}$ values for these vents suggest a non-zero endmember sulfate concentration (Section 4.1). Here, we can apply a similar explanation as Sakai et al. (1990) and Gamo et al. (1991). In their work, measured concentrations of the vent fluids from the moderate temperature CLAM site also line up with a zero-Mg and zero-sulfate endmember, but non-seawater $\delta^{34}S_{sulfate}$ indicates a sulfate component that is not derived from ambient seawater. For the measured compositions to plot along the zero-Mg, zero-sulfate mixing line, Sakai et al. (1990) suggested that "the CLAM solution should also contain a corresponding amount of Mg and therefore its composition cannot be estimated by simple extrapolation to Mg = 0". Here, we suggest the use of Sr isotope ratios to correct for seawater entrainment during sampling. Sr isotopes behave conservatively upon mixing between seawater and LCHF endmember fluid and thus can be used as an alternative for Mg. All endmember vent fluid compositions presented in the manuscript, unless stated otherwise, are corrected by extrapolation to an endmember $^{87}Sr/^{86}Sr$ ratio of 0.70650 (Table 2).

The Sr isotope ratio of any fluid sample, $^{87}Sr/^{86}Sr_{sample}$, can be described by the following mass balance relationship (Faure, 1986):

$$\frac{^{87}Sr}{^{86}Sr_{sample}} = \frac{\%SW_{Sr}[Sr]_{SW}\left(\frac{^{87}Sr}{^{86}Sr_{SW}}\right) + (100 - \%SW_{Sr})[Sr]_{HT}\left(\frac{^{87}Sr}{^{86}Sr_{HT}}\right)}{\%SW_{Sr}[Sr]_{SW} + (100 - \%SW_{Sr})[Sr]_{HT}} \quad \text{(A1)}$$

where:

$\%SW_{Sr}$ is the weight percent of seawater entrained in the sample during sampling;

$[Sr]_{SW}$ is the Sr concentration of seawater;

$[Sr]_{HT}$ is the Sr concentration of pure hydrothermal fluid;

$\frac{^{87}Sr}{^{86}SrSW}$ is the Sr isotope ratio of seawater; and.

$\frac{^{87}Sr}{^{86}SrHT}$ is the Sr isotope ratio of pure hydrothermal fluid.

Equation A(1) can be re-arranged to solve for $\%SW_{Sr}$ for any given sample:

$$\%SW_{Sr} = \frac{[Sr]_{HT}\left(\frac{^{87}Sr}{^{86}Sr_{HT}} - \frac{^{87}Sr}{^{86}Sr_{sample}}\right)}{[Sr]_{HT}\left(\frac{^{87}Sr}{^{86}Sr_{HT}} - \frac{^{87}Sr}{^{86}Sr_{sample}}\right) + [Sr]_{SW}\left(\frac{^{87}Sr}{^{86}Sr_{sample}} - \frac{^{87}Sr}{^{86}Sr_{SW}}\right)} \times 100\%. \quad \text{(A2)}$$

Similar to the zero Mg approach, measured concentrations can be plotted against calculated $\%SW_{Sr}$, and endmember compositions correspond to values where the regression line intercepts $\%SW_{Sr} = 0$. Since two component mixing lines of isotopic compositions are not linear when plotted against concentrations or %SW (e.g., Fig. 2C), except in the case where $[Sr]_{HT} = [Sr]_{SW}$, endmember isotopic compositions were calculated using an isotope mass balance approach.

If we compare the weight fractions of seawater derived from Mg ($\%SW_{Mg}$) and those derived from Sr isotopes ($\%SW_{Sr}$) for the HOG samples (Table 2), we find that in some vent fluids $\%SW_{Mg}$ is greater than or equal to $\%SW_{Sr}$, with differences (ΔSW) of up to 5%. This difference is more pronounced in the vents with temperatures<70 °C. The zero-Mg approach generates lower calculated concentrations of endmember SO_4^{2-} than the Sr-isotope approach (Fig. A1).

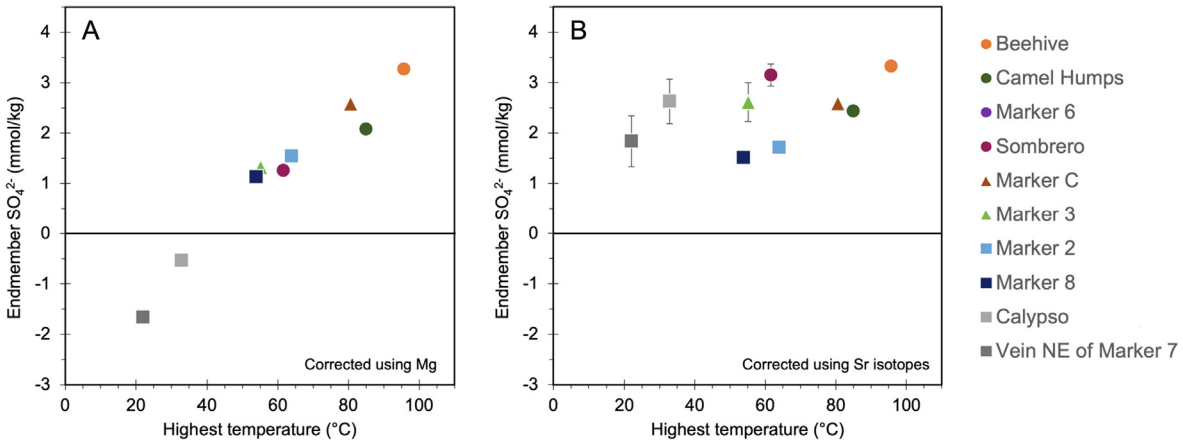

Fig. A1. Endmember sulfate concentrations at (A) zero-Mg and (B) at $^{87}Sr/^{86}Sr = 0.70650$ plotted against highest measured vent temperatures. At zero-Mg, endmember sulfate compositions are lower than at $^{87}Sr/^{86}Sr = 0.70650$.

APPENDIX B. SUPPLEMENTARY MATERIAL

Supplementary material to this article can be found online at https://doi.org/10.1016/j.gca.2022.06.027.

REFERENCES

Albarède F., Michard A., Minster J. F. and Michard G. (1981) $^{87}Sr/^{86}Sr$ ratios in hydrothermal waters and deposits from the East Pacific Rise at 21°N. *Earth Planet. Sci. Lett.* **55**, 229–236.

Allen D. E. and Seyfried W. E. (2004) Serpentinization and heat generation: Constraints from Lost City and Rainbow hydrothermal systems. *Geochim. Cosmochim. Acta* **68**, 1347–1354.

Alt J. C., Schwarzenbach E. M., Früh-Green G. L., Shanks W. C., Bernasconi S. M., Garrido C. J., Crispini L., Gaggero L., Padrón-Navarta J. A. and Marchesi C. (2013) The role of serpentinites in cycling of carbon and sulfur: Seafloor serpentinization and subduction metamorphism. *Lithos* **178**, 40–54.

Alt J. C. and Shanks W. C. (1998) Sulfur in serpentinized oceanic peridotites: Serpentinization processes and microbial sulfate reduction. *J. Geophys. Res. Solid Earth* **103**, 9917–9929.

Amend J. P., McCollom T. M., Hentscher M. and Bach W. (2011) Catabolic and anabolic energy for chemolithoautotrophs in deep-sea hydrothermal systems hosted in different rock types. *Geochim. Cosmochim. Acta* **75**, 5736–5748.

Berndt M. E., Seyfried W. E. and Beck J. W. (1988) Hydrothermal alteration processes at midocean ridges: experimental and theoretical constraints from Ca and Sr exchange reactions and Sr isotopic ratios. *J. Geophys. Res.* **93**, 4573–4583.

Bethke C. M., Farrel B. and Sharifi M. (2020) *GWB Essentials Guide.*. Aqueous Solutions, LLC Champaign, Illinois.

Bischoff J. L. and Dickson F. W. (1975) Seawater-basalt interaction at 200°C and 500 bars: Implications for origin of sea-floor heavy-metal deposits and regulation of seawater chemistry. *Earth Planet. Sci. Lett.* **25**, 385–397.

Boschi C., Dini A., Früh-Green G. L. and Kelley D. S. (2008) Isotopic and element exchange during serpentinization and metasomatism at the Atlantis Massif (MAR 30°N): Insights from B and Sr isotope data. *Geochim. Cosmochim. Acta* **72**, 1801–1823.

Boschi C., Früh-Green G. L., Delacour A., Karson J. A. and Kelley D. S. (2006) Mass transfer and fluid flow during detachment faulting and development of an oceanic core complex, Atlantis Massif (MAR 30°N). *Geochem. Geophys. Geosyst.* **7**.

Bradley A. S. and Summons R. E. (2010) Multiple origins of methane at the Lost City Hydrothermal Field. *Earth Planet. Sci. Lett.* **297**, 34–41.

Brazelton W. J., Ludwig K. A., Sogin M. L., Andreishcheva E. N., Kelley D. S., Shen C. C., Edwards R. L. and Baross J. A. (2010) Archaea and bacteria with surprising microdiversity show shifts in dominance over 1,000-year time scales in hydrothermal chimneys. *Proc. Natl. Acad. Sci. U. S. A.* **107**, 1612–1617.

Brazelton W. J., Schrenk M. O., Kelley D. S. and Baross J. A. (2006) Methane- and sulfur-metabolizing microbial communities dominate the lost city hydrothermal field ecosystem. *Appl. Environ. Microbiol.* **72**, 6257–6270.

Brunner B. and Bernasconi S. M. (2005) A revised isotope fractionation model for dissimilatory sulfate reduction in sulfate reducing bacteria. *Geochim. Cosmochim. Acta* **69**, 4759–4771.

Butterfield D. A. and Massoth G. J. (1994) Geochemistry of north Cleft segment vent fluids: temporal changes in chlorinity and their possible relation to recent volcanism. *J. Geophys. Res.* **99**, 4951–4968.

Charlou J. L., Donval J. P., Fouquet Y., Jean-Baptiste P. and Holm N. (2002) Geochemistry of high H2 and CH4 vent fluids issuing from ultramafic rocks at the Rainbow hydrothermal field (36°14′N, MAR). *Chem. Geol.* **191**, 345–359.

Charlou J. L., Fouquet Y., Bougault H., Donval J. P., Etoubleau J., Jean-Baptiste P., Dapoigny A., Appriou P. and Rona P. A. (1998) Intense CH4 plumes generated by serpentinization of ultramafic rocks at the intersection of the 15°20'N fracture zone and the Mid-Atlantic Ridge. *Geochim. Cosmochim. Acta* **62**, 2323–2333.

Coggon R. M. and Teagle D. A. H. (2011) Hydrothermal calcium-carbonate veins reveal past ocean chemistry. *TrAC - Trends Anal. Chem.* **30**, 1252–1268.

Von Damm K. L., Edmond J. M., Measures C. I. and Grant B. (1985) Chemistry of submarine hydrothermal solutions at Guaymas Basin. *Gulf of California. Geochim. Cosmochim. Acta* **49**, 2221–2237.

Delacour A., Früh-Green G. L. and Bernasconi S. M. (2008a) Sulfur mineralogy and geochemistry of serpentinites and gabbros of the Atlantis Massif (IODP Site U1309). *Geochim. Cosmochim. Acta* **72**, 5111–5127.

Delacour A., Früh-Green G. L., Bernasconi S. M. and Kelley D. S. (2008b) Sulfur in peridotites and gabbros at Lost City (30°N,

MAR): Implications for hydrothermal alteration and microbial activity during serpentinization. *Geochim. Cosmochim. Acta* **72**, 5090–5110.

Delacour A., Früh-Green G. L., Bernasconi S. M., Schaeffer P. and Kelley D. S. (2008c) Carbon geochemistry of serpentinites in the Lost City Hydrothermal System (30°N, MAR). *Geochim. Cosmochim. Acta* **72**, 3681–3702.

Delacour A., Früh-Green G. L., Frank M., Gutjahr M. and Kelley D. S. (2008d) Sr- and Nd-isotope geochemistry of the Atlantis Massif (30°N, MAR): Implications for fluid fluxes and lithospheric heterogeneity. *Chem. Geol.* **254**, 19–35.

Deniel C. and Pin C. (2001) Single-stage method for the simultaneous isolation of lead and strontium from silicate samples for isotopic measurements. *Anal. Chim. Acta* **426**, 95–103.

Detmers J., Brüchert V., Habicht K. S. and Kuever J. (2001) Diversity of Sulfur Isotope Fractionations by Sulfate-Reducing Prokaryotes. *Appl. Environ. Microbiol.* **67**, 888–894.

Eickenbusch P., Takai K., Sissman O., Suzuki S., Menzies C., Sakai S., Sansjofre P., Tasumi E., Bernasconi S. M., Glombitza C., Jørgensen B. B., Morono Y. and Lever M. A. (2019) Origin of short-chain organic acids in serpentinite mud volcanoes of the Mariana convergent margin. *Front. Microbiol.* **10**, 1–21.

Elsgaard L., Isaksen M. A. I. F., Rgensen B. B. J., Alayse A., Jannasch H. W., de Roscoff S. B., Pierre U. and Roscoff F. (1994) Microbial sulfate reduction in deep-sea sediments at the Guaymas Basin hydrothermal vent area: Influence of temperature and substrates. *Geochim. Cosmochim. Acta* **58**, 3335–3343.

Epstein S. and Mayeda T. (1953) Variation of O18 content of waters from natural sources. *Geochim. Cosmochim. Acta* **4**, 213–224.

Faure G. (1986) Isotope systematics of two-component mixtures. In *Principles of Isotope Geology*. John Wiley and Sons, Inc., pp. 141–153.

Foustoukos D. I., Savov I. P. and Janecky D. R. (2008) Chemical and isotopic constraints on water/rock interactions at the Lost City hydrothermal field, 30°N Mid-Atlantic Ridge. *Geochim. Cosmochim. Acta* **72**, 5457–5474.

Früh-Green G. L., Kelley D. S., Bernasconi S. M., Karson J. A., Ludwig K. A., Butterfield D. A., Boschi C. and Proskurowski G. (2003) 30,000 Years of hydrothermal activity at the Lost City vent field. *Science* **301**, 495–498.

Früh-Green G. L., Orcutt B. N., Rouméjon S., Lilley M. D., Morono Y., Cotterill C., Green S., Escartin J., John B. E., McCaig A. M., Cannat M., Ménez B., Schwarzenbach E. M., Williams M. J., Morgan S., Lang S. Q., Schrenk M. O., Brazelton W. J., Akizawa N., Boschi C., Dunkel K. G., Quéméneur M., Whattam S. A., Mayhew L., Harris M., Bayrakci G., Behrmann J. H., Herrero-Bervera E., Hesse K., Liu H. Q., Ratnayake A. S., Twing K., Weis D., Zhao R. and Bilenker L. (2018) Magmatism, serpentinization and life: Insights through drilling the Atlantis Massif (IODP Expedition 357). *Lithos* **323**, 137–155.

Gamo T., Sakai H., Kim E. S., Shitashima K., Ishibashi J. and ichiro, (1991) High alkalinity due to sulfate reduction in the CLAM hydrothermal field. *Okinawa Trough. Earth Planet. Sci. Lett.* **107**, 328–338.

Gerasimchuk A. L., Shatalov A. A., Novikov A. L., Butorova O. P., Pimenov N. V., Lein A. Y., Yanenko A. S. and Karnachuk O. V. (2010) The search for sulfate-reducing bacteria in mat samples from the lost city hydrothermal field by molecular cloning. *Microbiology* **79**, 96–105.

German C. R. and Von Damm K. L. (2003) Hydrothermal Processes. *Treatise on. Geochemistry* **6–9**, 181–222.

Hoek J., Reysenbach A. L., Habicht K. S. and Canfield D. E. (2006) Effect of hydrogen limitation and temperature on the fractionation of sulfur isotopes by a deep-sea hydrothermal vent sulfate-reducing bacterium. *Geochim. Cosmochim. Acta* **70**, 5831–5841.

Jørgensen B. B., Isaksen M. F. and Jannasch H. W. (1992) Bacterial sulfate reduction above 100°C in deep-sea hydrothermal vent sediments. *Science* **80). 258**, 1756–1757.

Kajiwara Y. and Krouse H. R. (1971) Sulfur Isotope Partitioning in Metallic Sulfide Systems. *Can. J. Earth Sci.* **8**, 1397–1408.

Kelley D. S. and Früh-Green G. L. (1999) Abiogenic methane in deep-seated mid-ocean ridge environments: Insights from stable isotope analyses. *J. Geophys. Res. Earth* **104**, 10439–10460.

Kelley D. S. and Früh-Green G. L. (2001) *Volatiles in mid-ocean ridge environments*. Geol. Soc. Am. Spec. Pap., pp. 237–260.

Kelley D. S., Karson J. A., Blackman D. K., Früh-Green G. L., Butterfield D. A., Lilley M. D., Olson E. J., Schrenk M. O., Roe K. K., Lebon G. T. and Rivizzigno P. (2001) An off-axis hydrothermal vent field near the mid-atlantic ridge at 30°N. *Nature* **412**, 145–149.

Kelley D. S., Karson J. A., Früh-Green G. L., Yoerger D. R., Shank T. M., Butterfield D. A., Hayes J. M., Schrenk M. O., Olson E. J., Proskurowski G., Jakuba M., Bradley A. S., Larson B., Ludwig K., Glickson D., Buckman K., Bradley A. S., Brazelton W. J., Roe K., Elend M. J., Delacour A., Bernasconi S. M., Lilley M. D., Baross J. A., Summons R. E. and Sylva S. P. (2005) A serpentinite-hosted ecosystem: The Lost City hydrothermal field. *Science* **307**, 1428–1434.

Kemp A. L. W. and Thode H. G. (1968) The mechanism of the bacterial reduction of sulphate and of sulphite from isotope fractionation studies. *Geochim. Cosmochim. Acta* **32**, 71–91.

Kiyosu Y. (1980) Chemical reduction and sulfur-isotope effects of sulfate by organic matter under hydrothermal conditions. *Chem. Geol.* **30**, 47–56.

Kiyosu Y. and Krouse R. H. (1990) The role of organic and acid the in the sulfur abiogenic isotope reduction effect. *Geochem. J.* **24**, 21–27.

Klein F., Grozeva N. G. and Seewald J. S. (2019) Abiotic methane synthesis and serpentinization in olivine-hosted fluid inclusions. *Proc. Natl. Acad. Sci. U. S. A.* **116**, 17666–17672.

Klein F., Humphris S. E. and Bach W. (2020) Brucite formation and dissolution in oceanic serpentinite. *Geochemical Perspect. Lett.*, 1–5.

Konn C., Charlou J. L., Holm N. G. and Mousis O. (2015) The production of methane, hydrogen, and organic compounds in ultramafic-hosted hydrothermal vents of the mid-atlantic ridge. *Astrobiology* **15**, 381–399.

Kuhn T., Herzig P. M., Hannington M. D., Garbe-Schönberg D. and Stoffers P. (2003) Origin of fluids and anhydrite precipitation in the sediment-hosted Grimsey hydrothermal field north of Iceland. *Chem. Geol.* **202**, 5–21.

Labidi J., Young E. D. D., Giunta T., Kohl I. E. E., Seewald J., Tang H., Lilley M. D. D. and Früh-Green G. L. L. (2020) Methane thermometry in deep-sea hydrothermal systems: evidence for re-ordering of doubly-substituted isotopologues during fluid cooling. *Geochim. Cosmochim. Acta* **288**, 248–261.

Lang S. Q. and Benitez-Nelson B. (2021) Hydrothermal Organic Geochemistry (HOG) sampler for deployment on deep-sea submersibles. *Deep Sea Res. Part I Oceanogr. Res. Pap.* **173** 103529.

Lang S. Q. and Brazelton W. J. (2020) Habitability of the marine serpentinite subsurface: a case study of the Lost City hydrothermal field. *Philos. Trans. A. Math. Phys. Eng. Sci.* **378**, 20180429.

Lang S. Q., Butterfield D. A., Schulte M., Kelley D. S. and Lilley M. D. (2010) Elevated concentrations of formate, acetate and dissolved organic carbon found at the Lost City hydrothermal field. *Geochim. Cosmochim. Acta* **74**, 941–952.

Lang S. Q., Früh-Green G. L., Bernasconi S. M., Brazelton W. J., Schrenk M. O. and McGonigle J. M. (2018) Deeply-sourced

formate fuels sulfate reducers but not methanogens at Lost City hydrothermal field. *Sci. Rep.* **8**, 1–10.

Lang S. Q., Früh-Green G. L., Bernasconi S. M., Lilley M. D., Proskurowski G., Méhay S. and Butterfield D. A. (2012) Microbial utilization of abiogenic carbon and hydrogen in a serpentinite-hosted system. *Geochim. Cosmochim. Acta* **92**, 82–99.

Liebmann J., Schwarzenbach E. M., Früh-Green G. L., Boschi C., Rouméjon S., Strauss H., Wiechert U. and John T. (2018) Tracking Water-Rock Interaction at the Atlantis Massif (MAR, 30°N) Using Sulfur Geochemistry. *Geochemistry*. *Geophys. Geosystems* **19**, 4561–4583.

Lowell R. P. (2017) A fault-driven circulation model for the Lost City Hydrothermal Field. *Geophys. Res. Lett.* **44**, 2703–2709.

Ludwig K. A., Kelley D. S., Butterfield D. A., Nelson B. K., Früh-Green G., Fru G. and Früh-Green G. (2006) Formation and evolution of carbonate chimneys at the Lost City Hydrothermal Field. *Geochim. Cosmochim. Acta* **70**, 3625–3645.

Machel H. G. (2001) Bacterial and thermochemical sulfate reduction in diagenetic settings - old and new insights. *Sediment. Geol.* **140**, 143–175.

Machel H. G. (1998) Gas souring by thermochemical sulfate reduction at 140°C: Discussion. *Am. Assoc. Pet. Geol. Bull.* **82**, 1870–1873.

Machel H. G., Krouse H. R. and Sassen R. (1995) Products and distinguishing criteria of bacterial and thermochemical sulfate reduction. *Appl. Geochemistry* **10**, 373–389.

McCollom T. M. (2007) Geochemical Constraints on Sources of Metabolic Energy for Chemolithoautotrophy in Ultramafic-Hosted Deep-Sea Hydrothermal Systems. *Astrobiology* **7**, 933–950.

McDermott J. M., Seewald J. S., German C. R. and Sylva S. P. (2015) Pathways for abiotic organic synthesis at submarine hydrothermal fields. *Proc. Natl. Acad. Sci.* **112**, 7668–7672.

McDonough W. F. (1990) Constraints on the composition of the continental lithospheric mantle. *Earth Planet. Sci. Lett.* **101**, 1–18.

Monnin C., Chavagnac V., Boulart C., Ménez B., Gérard M., Gérard E., Pisapia C., Quéméneur M., Erauso G., Postec A., Guentas-Dombrowski L., Payri C. and Pelletier B. (2014) Fluid chemistry of the low temperature hyperalkaline hydrothermal system of Prony bay (New Caledonia). *Biogeosciences* **11**, 5687–5706.

Mottl M. J. and Holland H. D. (1978) Chemical exchange during hydrothermal alteration of basalt by seawater-I. Experimental results for major and minor components of seawater. *Geochim. Cosmochim. Acta* **42**, 1103–1115.

Mottl M. J., Holland H. D. and Corr R. F. (1979) Chemical exchange during hydrothermal alteration of basalt by seawater-II. Experimental results for Fe, Mn, and sulfur species. *Geochim. Cosmochim. Acta* **43**, 869–884.

Nier A. O. (1938) The Isotopic Constitution of Strontium, Barium, Bismuth, Thallium and Mercury. *Phys. Rev.* **54**, 275–278.

Ohmoto H. (1972) Systematics of sulfur and carbon isotopes in hydrothermal ore deposits. *Econ. Geol.* **67**, 551–578.

Ohmoto H. and Lasaga A. C. (1982) Kinetics of reactions between aqueous sulfates and sulfides in hydrothermal systems. *Geochim. Cosmochim. Acta* **46**, 1727–1745.

Ohmoto H. and Rye R. O. (1979) Isotopes of sulphur and carbon. In *Geochemistry of hydrothermal ore deposits* (ed. H. L. Barnes). John Wiley and Sons Inc, New York, pp. 509–567.

Palmer M. R. and Edmond J. M. (1989) The strontium isotope budget of the modern ocean. *Earth Planet. Sci. Lett.* **92**, 11–26.

Postgate J. R. (1984) *The Sulfate-reducing Bacteria*, 2nd ed. Cambridge University Press, Cambridge.

Proskurowski G., Lilley M. D., Kelley D. S. and Olson E. J. (2006) Low temperature volatile production at the Lost City Hydrothermal Field, evidence from a hydrogen stable isotope geothermometer. *Chem. Geol.* **229**, 331–343.

Proskurowski G., Lilley M. D., Seewald J. S., Früh-Green G. L., Olson E. J., Lupton J. E., Sylva S. P. and Kelley D. S. (2008) Abiogenic hydrocarbon production at lost city hydrothermal field. *Science* **319**, 604–607.

Raab M. and Spiro B. (1991) Sulfur isotopic variations during seawater evaporation with fractional crystallization. *Chem. Geol. Isot. Geosci. Sect.* **86**, 323–333.

Reed B. C. (2010) A spreadsheet for linear least-squares fitting with errors in both coordinates. *Phys. Educ.* **45**, 93–96.

Rees C. E., Jenkins W. J. and Monster J. (1978) The sulphur isotopic composition of ocean water sulphate. *Geochim. Cosmochim. Acta* **42**, 377–381.

Reeves E. P., McDermott J. M. and Seewald J. S. (2014) The origin of methanethiol in midocean ridge hydrothermal fluids. *Proc. Natl. Acad. Sci. U. S. A.* **111**, 5474–5479.

Rouméjon S., Früh-Green G. L., Orcutt B. N., Green S., Cotterill C., Morgan S., Akizawa N., Bayrakci G., Behrmann J. H., Herrero-Bervera E., Boschi C., Brazelton W., Cannat M., Dunkel K. G., Escartin J., Harris M., Hesse K., John B., Lang S. Q., Lilley M., Liu H. Q., Mayhew L., McCaig A., Menez B., Morono Y., Quéméneur M., Ratnayake A. S., Schrenk M., Schwarzenbach E., Twing K., Weis D., Whattam S. A., Williams M. and Zhao R. (2018a) Alteration Heterogeneities in Peridotites Exhumed on the Southern Wall of the Atlantis Massif (IODP Expedition 357). *J. Petrol.* **59**, 1–29.

Rouméjon S., Williams M. J. and Früh-Green G. L. (2018b) In-situ oxygen isotope analyses in serpentine minerals: Constraints on serpentinization during tectonic exhumation at slow- and ultraslow-spreading ridges. *Lithos* **323**, 156–173.

Russell M. J., Hall A. J. and Martin W. (2010) Serpentinization as a source of energy at the origin of life. *Geobiology* **8**, 355–371.

Saccocia P. J., Seewald J. S. and Shanks W. C. (2009) Oxygen and hydrogen isotope fractionation in serpentine-water and talc-water systems from 250 to 450 °C, 50 MPa. *Geochim. Cosmochim. Acta* **73**, 6789–6804.

Sakai H. (1968) Isotopic properties of sulfur compounds in hydrothermal processes. *Geochem. J.* **2**, 29–49.

Sakai H., Gamo T., Kim E.-S., Shitashima K., Yanagisawa F., Tsutsumi M., Ishibashi J., Sano Y., Wakita H., Tanaka T., Matsumoto T., Naganuma T. and Mitsuzawa K. (1990) Unique chemistry of the hydrothermal solution in the mid-Okinawa Trough Backarc Basin. *Geophys. Res. Lett.* **17**, 2133–2136.

Sakai H., Marais D. J. D., Ueda A. and Moore J. G. (1984) Concentrations and isotope ratios of carbon, nitrogen and sulfur in ocean-floor basalts. *Geochim. Cosmochim. Acta* **48**, 2433–2441.

Salters V. J. M. and Stracke A. (2004) Composition of the depleted mantle. *Geochemistry*. *Geophys. Geosystems* **5**, 1–27.

Schmidt K., Koschinsky A., Garbe-Schönberg D., de Carvalho L. M. and Seifert R. (2007) Geochemistry of hydrothermal fluids from the ultramafic-hosted Logatchev hydrothermal field, 15°N on the Mid-Atlantic Ridge: Temporal and spatial investigation. *Chem. Geol.* **242**, 1–21.

Schrenk M. O., Kelley D. S., Bolton S. A., Baross J. A., Ridge M., Schrenk M. O., Kelley D. S., Bolton S. A. and Baross J. A. (2004) Low archaeal diversity linked to subseafloor geochemical processes at the Lost City Hydrothermal Field, Mid-Atlantic Ridge. *Environ. Microbiol.* **6**, 1086–1095.

Schulte M., Blake D., Hoehler T. and McCollom T. (2006) Early Earth and Mars. *Astrobiology* **6**, 364–376.

Seyfried W. E., Pester N. J., Tutolo B. M. and Ding K. (2015) The Lost City hydrothermal system: Constraints imposed by vent

fluid chemistry and reaction path models on subseafloor heat and mass transfer processes. *Geochim. Cosmochim. Acta* **163**, 59–79.

Shalev N., Bontognali T. R. R., Wheat C. G. and Vance D. (2019) New isotope constraints on the Mg oceanic budget point to cryptic modern dolomite formation. *Nat. Commun.* **10**, 1–10.

Shanks W. C. (2001) Stable isotopes in seafloor hydrothermal systems. *Rev. Mineral. Geochemistry* **43**, 469–526.

Shanks W. C., Böhlke J. K. and Seal R. R. (1995) Stable isotopes in mid-ocean ridge hydrothermal systems: Interactions between fluids, minerals, and organisms. *Geophys. Monogr. Ser.* **91**, 194–221.

Sim M. S., Ono S., Donovan K., Templer S. P. and Bosak T. (2011) Effect of electron donors on the fractionation of sulfur isotopes by a marine Desulfovibrio sp. *Geochim. Cosmochim. Acta* **75**, 4244–4259.

Sleep N. H. (1991) Hydrothermal circulation, anhydrite precipitation, and thermal structure at ridge axes. *J. Geophys. Res.* **96**, 2375–2387.

de Souza G. F., Reynolds B. C., Kiczka M. and Bourdon B. (2010) Evidence for mass-dependent isotopic fractionation of strontium in a glaciated granitic watershed. *Geochim. Cosmochim. Acta* **74**, 2596–2614.

Syverson D. D., Ono S., Shanks W. C. and Seyfried W. E. (2015) Multiple sulfur isotope fractionation and mass transfer processes during pyrite precipitation and recrystallization: An experimental study at 300 and 350°C. *Geochim. Cosmochim. Acta* **165**, 418–434.

Takai K., Nakamura K., Toki T., Tsunogai U., Miyazaki M., Miyazaki J., Hirayama H., Nakagawa S., Nunoura T. and Horikoshi K. (2008) Cell proliferation at 122°C and isotopically heavy CH4 production by a hyperthermophilic methanogen under high-pressure cultivation. *Proc. Natl. Acad. Sci. U. S. A.* **105**, 10949–10954.

Taylor H. P. (1977) Water/rock interactions and the origin of H2O in granitic batholiths. *J. Geol. Soc. London.* **133**, 509–558.

Templeton A. S. and Ellison E. T. (2020) Formation and loss of metastable brucite: does Fe(II)-bearing brucite support microbial activity in serpentinizing ecosystems? *Philos. Trans. A. Math. Phys. Eng. Sci.* **378**, 20180423.

Thirlwall M. F. (1991) Long-term reproducibility of multicollector Sr and Nd isotope ratio analysis. *Chem. Geol.* **94**, 85–104.

Wang D. T., Reeves E. P., McDermott J. M., Seewald J. S. and Ono S. (2018) Clumped isotopologue constraints on the origin of methane at seafloor hot springs. *Geochim. Cosmochim. Acta* **223**, 141–158.

Worden R. H., Smalley P. C. and Oxtoby N. H. (1995) Gas souring by thermochemical sulfate reduction at 140°C. *Am. Assoc. Pet. Geol. Bull.* **79**, 854–863.

Workman R. K. and Hart S. R. (2005) Major and trace element composition of the depleted MORB mantle (DMM). *Earth Planet. Sci. Lett.* **231**, 53–72.

Associate editor: Shuhei Ono